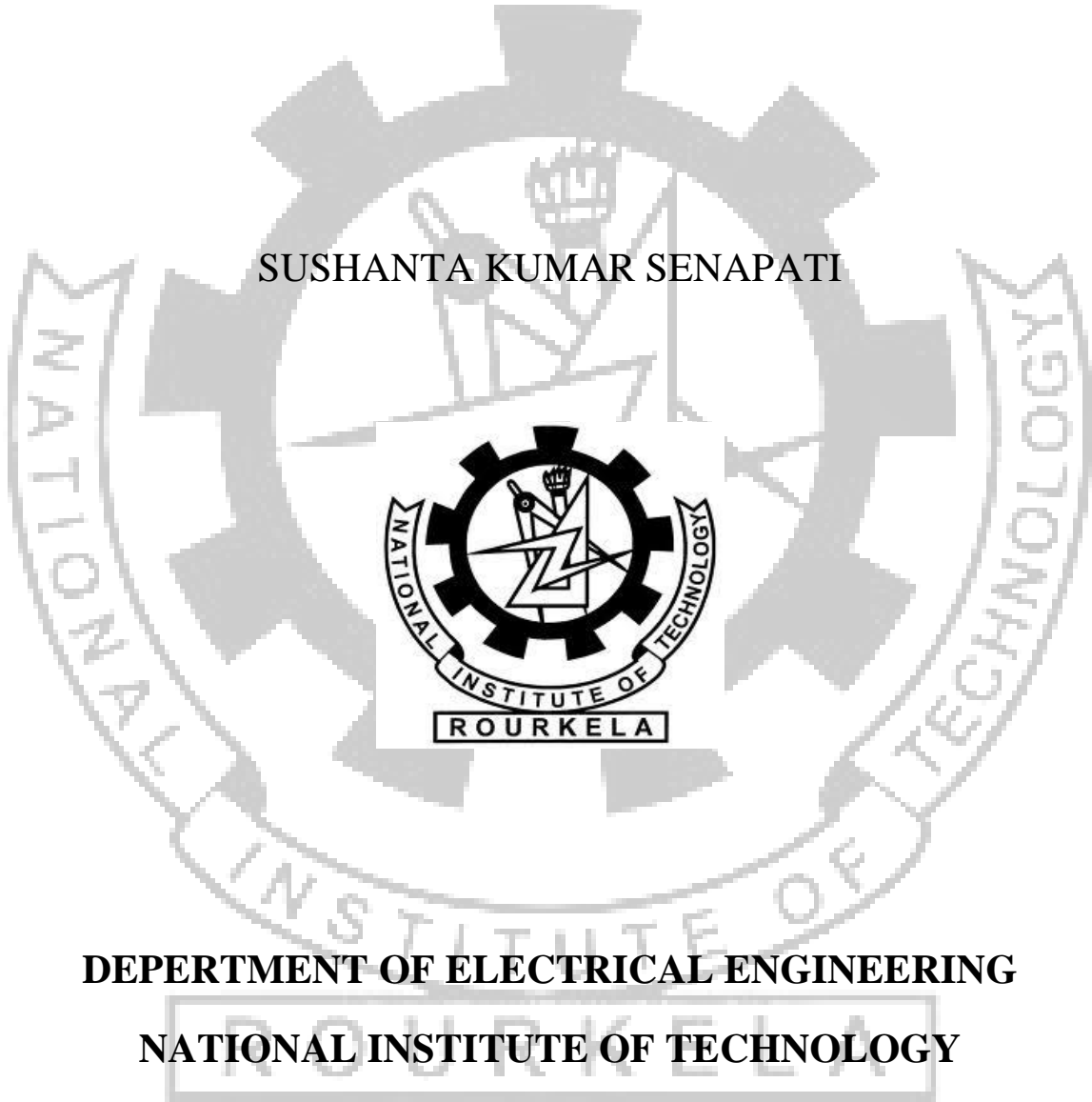# Modelling and Simulation of a Grid Connected Doubly Fed Induction Generator for Wind Energy Conversion System

SUSHANTA KUMAR SENAPATI

DEPERTMENT OF ELECTRICAL ENGINEERING

NATIONAL INSTITUTE OF TECHNOLOGY

ROURKELA -769008

Modelling and Simulation of a Grid Connected Doubly Fed Induction Generator for Wind Energy Conversion System

A Thesis

Submitted in partial fulfillment of the requirements

For the degree of

Master of Technology

In

Power electronics and drives

By

SUSHANTA KUMAR SENAPATI

Roll No. 212EE4255

Under the guidance of

Dr. Monalisa Pattnaik

DEPERTMENT OF ELECTRICAL ENGINEERING

NATIONAL INSTITUTE OF TECHNOLOGY

MAY 2014

NATIONAL INSTITUTE OF TECHNOLOGY

ROURKELA 769008

CERTIFICATE

I hereby certify that the work which is being presented in the thesis entitled "**Modelling and Simulation of a Grid Connected Doubly Fed Induction Generator for Wind Energy Conversion System**" in partial fulfilment of the requirements for the award of Master Of Technology Degree in Power Electronics & Drives submitted in Electrical Engineering at National Institute of Technology, Rourkela is an authentic record of my own work carried out under the supervision of Dr. Monalisa Pattnaik, Assistant Professor, PED. The matter presented in this thesis has not been submitted for the award of any other degree of this or any other university.

(Sushanta Kumar Senapati)

This is certify that the above statement made by candidate is correct and true to best of my knowledge.

(Dr. Monalisa Pattnaik)

Assistant Professor

Department of Electrical Engineering

National Institute of Technology, Rourkela

Rourkela -769008

ACKNOWLEDGMENTS

ABSTRACT

The Doubly Fed Induction Generator (DFIG) based wind turbine with variable-speed variable-pitch control scheme is the most popular wind power generator in the wind power industry. This machine can be operated either in grid connected or standalone mode. A thorough understanding of the modelling, control, and dynamic as well as the steady state analysis of this machine in both operation modes is necessary to optimally extract the power from the wind and accurately predict its performance. In this thesis, first a three phase PWM voltage source converter models expressed in the ABC and the DQO synchronous reference frame with its control schemes are developed and analysed. Then a DFIG-based wind turbine model connected to a constant voltage and frequency grid is developed in the Matlab/Simulink software in detail and its corresponding generator and turbine control structure is implemented. A thorough explanation of this control structure as well as the steady state behaviour of the overall wind energy conversion system which includes the aerodynamic models of the wind turbine, the DFIG models and the three-phase two-level PWM voltage source converter models are presented. A developed control schemes are also necessary to achieve useful output power from the WECS. These control schemes include the generator-side converter control, the grid-side converter control, the pitch angle control and the maximum power point tracking control. The grid-side converter controller is used to maintain the constant voltage across the capacitor and produce a unity power factor operation of the grid. The generator-side converter controller is used to regulating the torque, active power and reactive power. The maximum power point tracking control is used to provide the reference values for the active power at the stator terminals. The pitch angle control scheme is used to regulate the pitch angle and thus keep the output power at rated value even when the wind fluctuations.

TABLE OF CONTENTS

LIST OF FIGURES

LIST OF SYMBOLS

WECS	Wind energy conversion system
WTGS	Wind turbine generator system
DFIG	Doubly fed induction generator
PMSG	Permanent magnet synchronous generator
SCIG	Squirrel-cage induction generator
WRIG	Wound rotor induction generator
DFIM	Doubly fed induction machine
VSC	Voltage source converter
GSC	Grid side converter
RSC	Rotor side converter
MSC	Machine side converter
VSI	Voltage source inverter
PWM	Pulse width modulation
MPPT	Maximum power point tracking
FOC	Field oriented control
DTC	Direct torque control
DPC	Direct power control
IGBT	Insulated gate bipolar transistor
PI	Proportional and integral
UPF	Unity power factor
PLL	Phase locked loop

Chapter 1

Introduction

1.1 Background

With a society direction towards a future atmosphere disaster the demand for breakthrough inventions in green energy production has increased rapidly during the last periods. Solar cells, hydropower, bio fuels and wind turbines have all improved in performance and are sizing up.
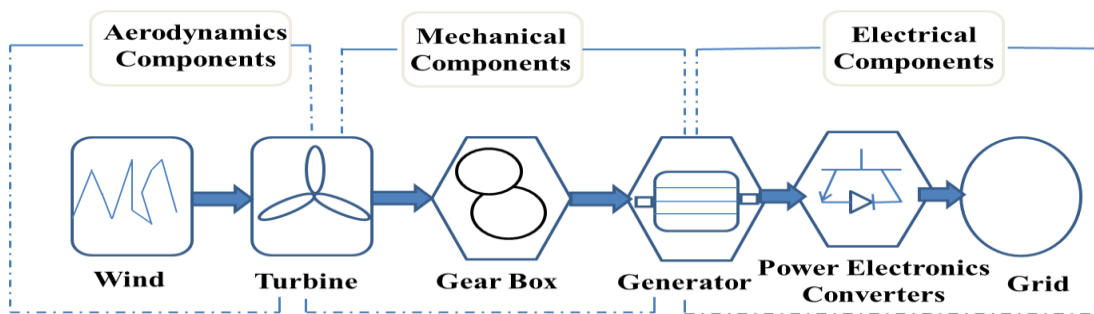
Figure 1.1 The components of WECS connected to grid [1]

The overall system of Wind Energy Conversion System (WECS) consisting of electro-mechanical and aerodynamic components which converts wind energy to electrical energy as shown in Figure 1.1 [1].

Due to environmental pollution, non-conventional energy sources being recognized in many countries by way of government-level policy. It is reported that by 2020, Europe will achieve 20% of power consumed in there supplying by large-scale offshore wind farms. Besides, Europe is now planning for enlarging the capacity of the large-scale offshore wind farms to more than 30 GW power by 2015 [2]. Besides Europe, other countries such as China and USA also have promising offshore wind power resources and similar plans for wind farm installation.

In the past years, energy generation from wind proficient a fast growing market. Therefore, in this thesis, the focus is put on the wind power generation as it is said to encounter large integration obstacles and possible solutions in the near future.

1.1.1 Components of a WTGS

The major components of a wind turbine-generator system (WTGS) are shown in Figure 1.2. The wind turbine (WT) is composed of three blades, the rotor hub and the nacelle located immediately behind the rotor hub which houses the gearbox, generator and other components.
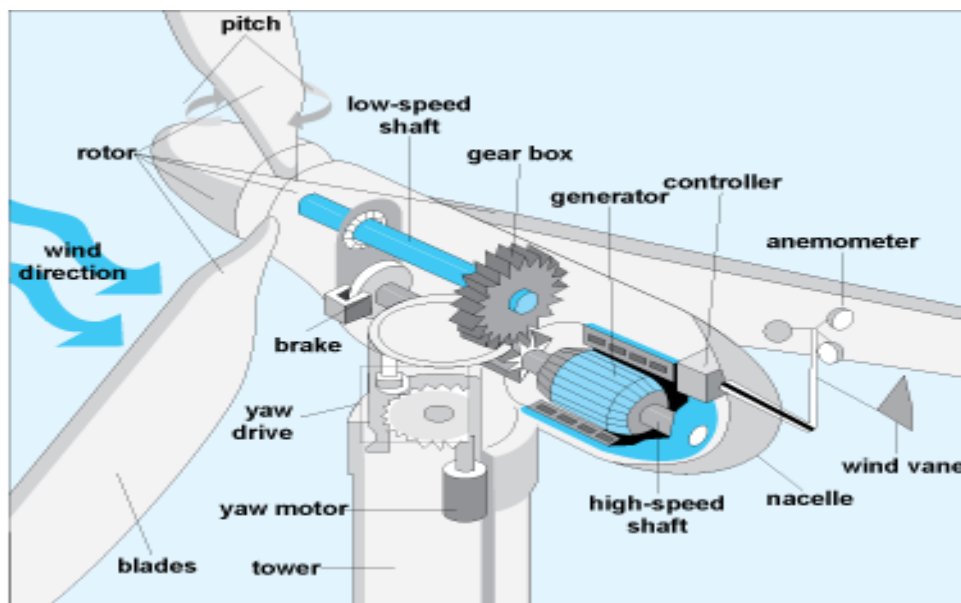
Figure 1.2 Components of a wind turbine-generator system [3]

The drive train system consists of three blades, a low-speed shaft, a gearbox, a high-speed shaft and a generator. The low-speed shaft connects the low-speed shaft to a two or three-stage gearbox, followed by a high-speed shaft connected to the generator [3]. The process of how the wind turbine system generates electrical power will be briefly summarized as follows: 1) when the flow of wind cross over the blades, causes them to rotate with the low-speed shaft , 2) the kinetic energy transferred from low-speed to high-speed rotating shaft through the gearbox, which step up the rotational speed, 3) the generator rotates at high speed nearer to the rated speed due to the high-speed shaft, 4) the revolving generator converts the mechanical energy to electrical energy.

Usually, the output voltages of the generator are low, and hence there will be the need for a transformer to step up the generator output voltage for the purpose of directly connecting to the grid.

Based on the wind direction, the yaw system will rotate the nacelle to make the wind turbine face into the wind. An emergency mechanical brake is equipped at the

high-speed shaft to protect the drive train system from the mechanical stress when experiencing wind gusts [4].

In addition, there are extensive on-board controllers that can change the pitch angle of the rotor blades, and regulate the yaw system and drive train system as well as power control components. Besides, these on-board controllers can break the rotor in possible runaway situations, such as high wind speeds and power-grid outages [3].

Other apparatuses of a wind turbine-generator system are wind vane, cooling fan and different sensors. These sensors include the anemometer, speed or position sensors as well as voltage and current sensors. The wind vane is used to measure the wind directions and then decide the operation of the yaw control system. Electric cooling fans are used to cool the gearbox, generator, power converters and the on-board controllers. The anemometer is used to measure the wind speed for tracking the maximum energy or protection purposes. For example, when the wind speed experiences gusts, the wind speed signal sensed by the anemometer will be sent to the on-board controllers, which will make the wind turbine shut down through the brake for safety considerations. Other sensors such as speed sensors and current sensors in wind turbine systems are used for control purposes, and should be specified according to the control schemes.

1.1.2 Wind Turbine Concepts

Generally speaking, wind power generation uses either fixed speed or variable speed turbines which can be characterised into four major types. The main changes between these wind turbine types are the ways how the aerodynamic efficiency of the rotor would be imperfect for different wind speed conditions. These four types are briefly described below [5]:

1. Fixed Speed Wind Turbines (WT Type A)

An asynchronous squirrel-cage induction generator (SCIG) directly connected to the grid via a transformer dealing with type 'A' wind turbine. The so-called "fix speed WT" comes from the point that the rotational speed of the wind turbine cannot be automatically controlled and will only differ by the wind speed. This type of wind turbine needs a switch to prevent motoring operation during low wind speeds, and also suffers a major drawback of reactive power consumption subsequently there is no reactive power regulator. Besides, this type of wind turbine transfers the wind variations

to mechanical instabilities and further converts these into electrical power oscillations due to the fact that there are no speed or torque control loops. These electrical power oscillations can lead to an effect in the case of a weak grid.

2. Partial Variable Speed Wind Turbine with Variable Rotor Resistance (WT Type B)

A wound rotor induction generator (WRIG) directly connected to the grid deals with this type of wind turbine. The controlled resistances are connected in series with the rotor phase windings of the generator. In this way, the total rotor resistances can be regulated, and thus the slip and the output power can be controlled. Due to the limitation of the serial resistance sizes, the variable speed range is usually small, typically 0-10% above synchronous speed [5].

3. Variable Speed Wind Turbine with Partial Scale Power Converter (WT Type C)

This arrangement, known as the doubly-fed induction generator (DFIG) concept, uses a variable speed controlled wind turbine. The stator phase windings of the doubly-fed induction generator are directly connected to the grid, while the rotor phase windings are connected to a back-to-back converter via slip rings. The power converters could control the rotor frequency and thus the rotor speed. The power rating of the power converters is typically rated ±30% around the rated power since the rotor of the DFIG would only deal with slip power. The smaller rating of the power converters makes this concept eye-catching from a cost-effective sight. Besides, this type of wind turbine can also achieve the desired reactive power compensation.

4. Variable Speed Wind Turbine with Full Scale Power Converter (WT Type D)

This structure usually uses a permanent magnet synchronous generator (PMSG) and a full-scale power converter. The stator phase windings are connected to the grid through a full-scale power converter. Some of this type of wind turbines adopt a gearless concept, which means that instead of connecting a gearbox to the generator, a direct driven multi-pole generator is used without a gearbox.

The first two types of wind turbines have many disadvantages. Examples of these disadvantages are: 1) they do not support any speed control, 2) they do not have reactive

compensation, 3) they require a stiff grid, 4) their mechanical structure must be able to support high mechanical stress caused by wind gusts, and so on. Therefore, this thesis does not show any detailed work about these considerations. The advantages and disadvantages of type C and type D wind turbine systems are summarized next.

Advantages of the DFIG-based WT generator scheme:

➢ It has the ability of decoupling the active and reactive power by adjusting the rotor terminal voltages. Hence, the power factor control can be implemented in this scheme.

➢ The DFIG is usually a wound rotor induction generator, which is simple in construction and cheaper than a PMSG.

➢ In a DFIG based wind turbine generator system, the power rating of the power converters is typically rated ±30% around the rated power, and this characteristic leads to many merits, such as, reduced converter cost, reduced filter volume and cost, less switching losses, less harmonic injections into the connected grid, and improved overall efficiency (approx. 2-3% more than full-scale frequency converter) if only the generator and power converters are considered [6].

Disadvantages of the DFIG-based wind turbine-generator system [4]:

❖ Needs slip-rings and gearbox, which will require frequent maintenance.

❖ Has limited fault ride through capability and needs protection schemes.

❖ Has complex control schemes.

Advantages of the PMSG based wind turbine generator system [7]:

➢ The PMSG can achieve full speed regulation.

➢ The PMSG makes it possible to avoid a gearbox, therefore, there are no mechanical stress issues when experiencing wind gusts.

➢ The PMSG does not need the slip-rings and brushes, hence, less maintenance will be needed. Therefore, a PMSG-based wind turbine will be more stable than a DFIG-based one.

➢ The PMSG can also attain the real power and reactive power control. The control schemes are relatively simple and easy to implement.

Disadvantages of the PMSG-based wind turbine-generator system [7] [8]:

❖ The power converters of a PMSG-based WTGS have a full-scale power rating, which means that the power converters will cause high losses, generate high harmonic components, and have high cost.

❖ The PMSG is usually a multi-polar generator, which is relatively large and heavy, and causes inconvenience for the installation.

❖ The PMSG naturally needs permanent magnets, which will increase the cost for this wind turbine concept considering the current market.

❖ The permanent magnets run the risk of demagnetization at high temperature.

Nowadays, DFIGs are most frequently used in the wind turbine industry for large wind turbines. Considering these merits of the DFIG-based wind turbine-generator systems, this thesis will only focus on DFIGs and then provide some detailed work about the modelling and control schemes of such wind turbine generator systems.

1.2 Literature Survey

In this section, a detailed literature review describing doubly-fed induction generator (DFIG) based wind turbine-generator systems will be presented. More specifically, the related previous studies and researches on the modelling, the control strategies, and the state of the art converter topologies applied in DFIG-based wind turbine-generator systems will be presented.

1.2.1 Modelling of a WTGS

As mentioned in last section, the modelling of a wind turbine generator system involves the aerodynamic modelling, the drive train system modelling, the DFIG modelling, and the power converter modelling, see Figure 1.1. Hence, this part of the study will only focus on the modelling of such system.

- Aerodynamic modelling

In [11], Tao sun deduced the maximum energy that a wind turbine system can extract from the air system under ideal conditions. In [12], the authors derived the relationship between the mechanical power input and the wind speed passing through a turbine rotor plane, which can be articulated by the power coefficient of the turbine. There are three most commonly used methods to simulate the power coefficient which is provided by the wind turbine manufacturer. The first two methods are given in references [11], [13] and [14]. The third method is the lookup table method, and given in references [10] and

[15]. There are two other methods to approximate the power efficiency curve, but they are not commonly used. Interested readers can find them in [16-17].

- Drive train modelling

For the drive train system modelling, the work in reference [18] elaborately explained the reduced mass conversion method and compared a six-mass model with reduced mass models for transient stability analysis. In [19], Stavros A. Papathanassiou used a six-mass drive train model to analyse the transient processes during faults and other disturbances. In [20], three different drive train models and different power electronic converter topologies were considered to study the harmonic assessment. In [18] and [23], the authors concluded that a two-mass drive train model was sufficient for transient analysis of WTGSs. Besides, the two-mass model is widely used in references [24-29]. Other references, such as [14, 30-33] focused their study on the generator control and modelling, where the drive train system was simply expressed by single mass models.

- DFIG modelling

The doubly-fed induction machines can be categorized into four types. These types are: the standard DFIM, the cascaded DFIM, the single-frame cascaded doubly-fed induction machine and the brushless DFIM [34]. However, only the standard type and brushless type of doubly-fed induction machines have been applied in wind turbine-generator systems. In reference [35], the authors developed the brushless DFIG by employing two cascaded induction machines to eliminate the brushes and copper rings, and used a closed-loop SFO control scheme to achieve active and reactive power control.

In [31] and [37], the authors adopted the synchronously rotating reference frame in order to simplify the controller design because of the fact that all the currents and voltages expressed under this reference frame will be of a dc nature. The DFIG model can usually be expressed by reduced order models, which can yield a third order model by neglecting the derivative terms of the stator flux and first order model by neglecting both the derivative terms of the stator flux and rotor flux [39]. But in [37], the authors proposed an enhanced

third order model which considered the dc-components of the stator currents, and gave a comparison between a full order model and the proposed model for wind ramp conditions. Alvaro Luna, in [40], deduced a new reduced third order model by ignoring the stator resistances and inductances through applying the Laplace transformation, and compared the proposed model with a full order model for transient analysis.

There are many references which made the comparison between the full order model and reduced order models [41-43]. In [44], the authors even considered the saturated conditions, and made a detailed comparison among these unsaturated and saturated full order models and reduced order models. Pablo Ledesma, in [45], compared a third order model with a full order model in two extreme operation points under short-circuit fault conditions. These points are sub-synchronous speed and super-synchronous speed, respectively. As known, the difference between the model of a SCIG and a DFIG is the rotor input. Hence, the simplified models of squirrel-cage induction generators may be helpful for understanding the reduced order models of DFIGs. Interested readers can find them in [46] and [47].

- Power converter modelling

    The traditional power converter used in wind turbine-generator systems is a back-to-back two-level PWM converter. The three-phase voltage source PWM converter model can be expressed in the ABC reference frame and the DQO synchronous reference frame which is deduced for control purposes. The mathematical model based on space vectors expressed in the ABC reference frame was derived in [48]. In [49-51], the authors showed the detailed work about the transformation of a PWM converter model from the ABC reference frame to the DQO synchronous reference frame. For wind turbine applications, some researchers simplified the power converter model by employing an equivalent ac voltage source that generates the fundamental frequency [32]. In [52], José R. Rodríguez gave the detailed description for the working principles, control strategies, and made comparisons for three-phase voltage source and current source PWM converters.

1.2.2 Control Strategies for a WTGS

The control schemes for a wind turbine-generator system include the pitch angle control, MPPT control, and the DFIG control. The traditional control techniques and advanced control techniques for wind turbine-generator systems are reviewed in this section.

1. Pitch angle control

There are numerous pitch angle regulation techniques described in the literatures [53-59]. The conventional pitch angle control usually uses PI controllers [53-55]. However, several advanced pitch control strategies were proposed. A new approach for the pitch angle control, which worked well for unstable and noisy circumstance, was presented in [56]. Besides, a fuzzy logic pitch angle controller was developed in [57], which did not need much knowledge about the system. Furthermore, a pitch angle controller using a generalized predictive control was presented in [58], whose strategy was based on the average wind speed and the standard deviation of the wind speed. Another pitch control scheme was proposed in [59], in which a self-tuning regulator adaptive controller that incorporated a hybrid controller of a linear quadratic Gaussian neuro-controller and a linear parameter estimator, was developed for the pitch angle control. In [60], the authors only applied a fuzzy logic pitch angle controller in a wind turbine-generator system to achieve the maximum power point tracking control and power control.

2. Maximum power point tracking control

To achieve the MPPT control, some regulator schemes have been presented. The maximum power point tracking control can be mainly divided into two types. They are the conventional control schemes and intelligent control schemes.

- Conventional control schemes

The conventional control schemes can also be divided into current mode control and speed mode control, which depends on the setting of reference values. The reference values are the active power and electromagnetic torque for current mode control [61-63], and the rotational speed for the speed mode control [64-65]. In [66], the author compared these two control strategies for

dynamic transient analysis, and concluded that the current mode control has slow response with simple construction, while the speed mode control has fast response with complex construction. The discussions and limitations of these two control schemes were presented in [67].

In fact, the wind speeds in above conventional control schemes need to be exactly measured. However, the anemometer cannot precisely measure the wind speed because of the flow misrepresentation, complex landscape and tower shadow influence [68]. Hence, some studies on maximum wind energy tracking without wind velocity measurement had been developed in [24], [69] and [70].

- Intelligent control

    The intelligent control strategies usually apply the hill-climbing control and the fuzzy logic control to the MPPT control. However, this control method is usually slow in speed because the step disturbance is fixed. Therefore, some improved hill-climbing control methods were proposed. For example, a method of using variable-step wind energy perturbation method to control the captured wind power was analysed in [67].

    Fuzzy logic control based MPPT strategies have the advantages of having robust speed control against wind gusts and turbine oscillatory torque, having superior dynamic and steady performances, and being independent of the turbine parameters and air density, see [68] and [73].

- Other control strategies

    In [74], the authors presented a novel adaptive MPPT control scheme in which the wind speed was projected by the output power and the productivity of the generator, and the maximum efficiency was estimated by the maximum tip-speed ratio tracker. A novel MPPT strategy that was proposed in [75], in which there was no requirement for the knowledge of wind turbine characteristic and measurements of the wind speed.

3. DFIG control

    Control of the DFIGs is more complex than the control of a squirrel-cage induction generator, because the DFIGs can operate at sub-synchronous speed

and super-synchronous speed by regulating the rotor terminal voltages. Through the years, many researchers have presented various types of DFIG control strategies, such as FOC, direct torque/power control, predictive control, sensor-less control and nonlinear control.

- Field oriented control

    Field oriented control (FOC) or vector control is commonly used in doubly-fed induction generator controls due to its ability of controlling the motor speed more efficiently, and the low economic cost to build an FOC system. Field oriented control also provides the ability of separately controlling the active and reactive power of the generator. Currently, there are mainly two types of field oriented control in DFIGs, which are stator voltage oriented control and stator flux oriented control, respectively.

- Direct torque/power control

    Recently, a new technique for directly control of the induction motors' torque or power was developed, which included direct torque control (DTC) and direct power control (DPC). Direct torque control scheme was first developed and presented by I. Takahashi and T. Nogouchi [79-80].

    Direct torque mechanism do not require current controllers, coordinate conversions, specific variations and current control loops [82]. Thus, direct torque control has the ability of directly controlling the rotor flux linkage magnitude and generator torque through properly selecting the inverter switching states [83]. To show the advantages of DTC, the comparison between the field oriented control and direct torque control was made in [84]. Direct torque control using space vector modulation technology was presented in [85]. In [86-88], the authors applied basic direct torque control to a doubly-fed induction generator. Direct torque control which was achieved without PI controller and only required the knowledge of grid voltages, rotor currents, and rotor position as was proposed in [82]. Z. Liu, in [89], proposed a novel direct torque control scheme which was developed based on the control of the rotor power factor. Direct power control has the merits of being simple, requiring

fewer sensors, having low computational complexity, fast transient response and low machine model dependency compared with direct torque control [90].

- Other control strategies

    In recent years, increasing attention is being paid to the application of predictive control in the field of the DFIG-based wind turbine-generator systems [86-88]. Several predictive direct power control strategies were studied and compared for ac/dc converters in [89]. Sensor-less control is usually achieved by estimating the rotor position, so that there is no need for the rotor position encoder. There are many studies worked on the sensor-less control, see reference [85-88].

1.3 Thesis organization

Including this introductory chapter, this thesis is organized in four chapters. In the second chapter, the modelling for a wind turbine-generator system is presented. More specifically, several methods to model the aerodynamics of a wind turbine rotor, the two-mass model and one-mass models for the drive train system, the detailed doubly-fed induction generator models expressed in the ABC reference frame and various DQO reference frames, and the PWM converter models expressed in the ABC and the DQO synchronous reference frame are developed and analysed. In Chapter 3, different control schemes for a wind turbine system are presented, which include the grid-side converter control, machine-side converter control. The simulation results as well as the corresponding analysis and discussion of these results will be also presented in this chapter. Finally, in Chapter 4, conclusions and recommendations will be presented.

Chapter 2

Modelling of a Wind Energy Conversion System

In wind energy conversion systems (WECSs), the kinetic wind energy is converted to electrical energy through doubly-fed induction generators (DFIGs) and then fed into the grid. In order to examine the power quality issues of variable speed wind turbine-generator systems, such as their interaction with the grid and different control scheme configurations, a proper model of the grid-connected variable speed WECS should be established first.

In this chapter, a general introduction to the WECSs is first given, in which a wind power conversion system is discussed briefly. Second, several methods of calculating the WECS captured power from the wind are proposed, which are the aerodynamic models of wind turbines. Second, a DFIG model expressed in the ABC reference frame is developed, and then several DFIG models expressed in various DQO-dqo reference frames are deduced from the ABC model by classical DQO transformations. Moreover, the reduced order models are also derived based on the DFIG model expressed in a synchronously rotating reference frame. Finally, the mathematical models of three-phase PWM voltage source converters are developed in the ABC reference frame and DQO synchronous reference frame.

2.1 Introduction

A variable speed wind turbine-generator system (WECS) schematic is shown in Figure 2.1. The stator phase windings of the doubly-fed induction generator (DFIG) are directly connected to the grid, while the rotor phase windings are connected to a bidirectional power converter via slip rings. The bidirectional power converter consists of two converters, i.e., grid side converter and rotor side converter, and between the two converters a dc-link capacitor is positioned. The main objective for the grid-side converter is to keep the variation of the dc-link voltage small. With control of the rotor side converter, it is possible to control the torque, the speed of the DFIG as well as its active and reactive power at the stator terminals.

Since the back-to-back power converters could be operated in bi-directional mode, the DFIG could thus be operated either in sub-synchronous speed mode or super-synchronous speed mode. Here, the speed range for the DFIG is around ±30% of the synchronous speed [10]. In this thesis, the model of the variable speed wind turbine with a DFIG was developed in a Matlab/Simulink environment.

Figure 2.1 DFIG based WECS scheme

2.2 Aerodynamic Model

A WTGS is an arrangement that converts the kinetic energy of the entering air flow into electrical energy. The transformation takes places by using two devices. The first one is the extraction device, which harvests the mechanical power by the wind flow turning the wind turbine rotor. The other one is the generator which transforms the rotational mechanical power to electrical power. The relationship between the mechanical input power and the wind speed passing through a turbine rotor plane can be written as follows [12]:

$$P_{wt} = \frac{1}{2}\rho\pi R^3 V_w^3 C_p(\lambda,\beta) \tag{2.1}$$

The tip speed ratio of a wind turbine is expressed as $\lambda = Rw_t/V_w$.

2.3 Back-to-back VSC Converters

These converters are consisting of a bidirectional voltage source converter connecting through the rotor of the generator and the grid as shown in Figure 2.2.

Basically these converters are made up of VSIs equipped with switches as IGBTs body diodes (see Figure 2.2), which permit a bi-directional current flow. Output switching harmonics of the GSC is diminished by the filters.
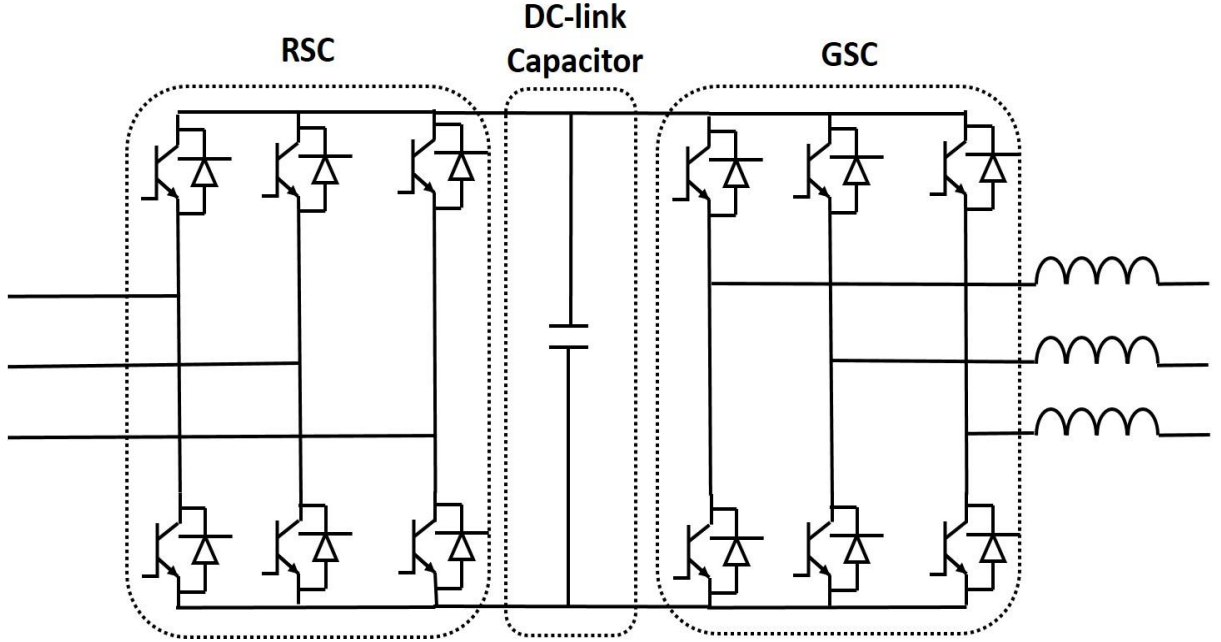
Figure 2.2 Power converter of the DFIG

2.4.1 Machine Side Converter

Power rating of the MSC is determined by two features, maximum slip power and reactive power control proficiency. To control the stator real power and reactive power independently are the main objectives of MSC.

2.4.2 Grid Side Converter

To minimize the switching losses in the GSC, it operates at UPF and its rating is obtained by maximum slip power [59]. The GSC is usually committed to controlling the dc-link voltage only. During a fault the converter is used to support grid reactive power [60]. The grid-side converter is used to boost grid power quality [61].

The amount of stored energy in the dc-link capacitor bank can be written as:

$$E_c = \int P dt = \frac{1}{2} C V_{dc}^2 \tag{2.2}$$

Where P the net power flow into the capacitor is, C is the dc-link capacitor value and V_{dc} is voltage across the capacitor. P is equal to $P_r - P_g$, where P_r is power flow into the rotor and P_g is power flow out of the grid.

2.5 Wind Speed Model

A wind speed signal produced by an autoregressive moving average (ARMA) model described in [62] is utilized in this simulation study, and its development is described here. The wind speed $V_{wind}(t)$ has two essential parts defined as [62]:

$$V_{wind}(t) = V_{w\_mean} + V_t(t) \tag{2.3}$$

Where V_{w_mean} is the mean wind speed and $V_t(t)$ is the instantaneous turbulent part, whose linear model is collected by Gaussian noise [62]:

$$\dot{V_t}(t) = -\frac{1}{T_w}V_t(t) + \alpha_t \tag{2.4}$$

The immediate turbulence section of wind speed is achieved as [62]:

$$V_t(t) = \sigma_t V_t \tag{2.5}$$

Where σ_t is the standard deviation and the ARMA time series model, which is expressed as [62]:

$$V_t(t) = aV_{t-1} - bV_{t-2} + cV_{t-3} + \alpha_t - d\alpha_{t-1} + e\alpha_{t-2} \tag{2.6}$$

Where a, b, and c are the autoregressive constraints, d and e are moving average parameters whose values being: a =1.7901, b=0.9087, c=0.0948, d=1.0929 and e =0.2892.
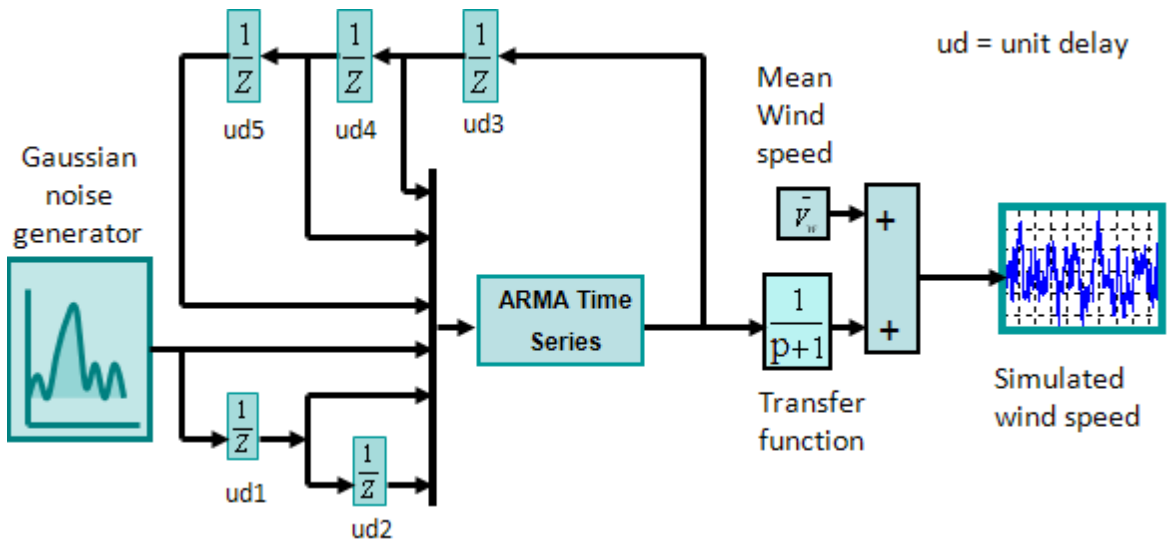
Figure 2.3 Wind speed generation by ARMA model in MATLAB/Simulink [62]
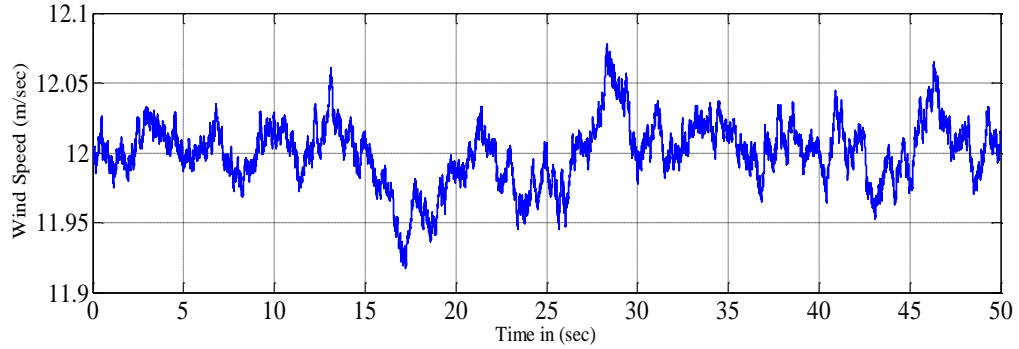
Figure 2.4 Sample wind speed (mean speed being 12 m/s) obtained using ARMA model

2.6   Doubly-Fed Induction Generator (DFIG) Models

For the purposes of better understanding and designing vector control schemes for a wind turbine-generator system, it is essential to know the dynamic model of the machine. A model of the electrical machine which is adequate for designing the control system must preferably include all the important dynamic effects arising during steady state and transient operations [126]. It should be effective for any arbitrary time variations of the voltages and currents generated by the converter which supplies the machine. In this section, such a model which is valid for any instantaneous variations of the voltages and currents, and can adequately describe the enactment of the machine under both steady state and transient operations, will be developed in both the ABC reference frame and several different DQO reference frames.

2.6.1   DFIG Model Expressed in the ABC Reference Frame

For simplicity, a wound rotor induction machine is considered with symmetrical two poles and three-phase windings. Figure 2.5 shows the cross sectional view of the machine under consideration, where the effects of slotting have been neglected.
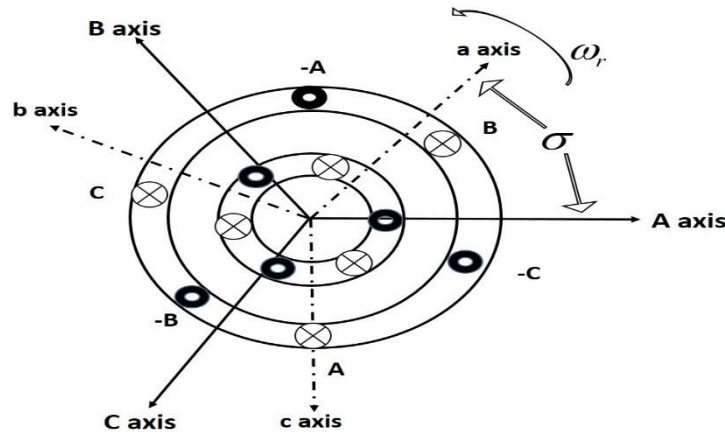
Figure 2.5 Cross sectional view of a wound rotor induction machine

In Figure 2.5, the stator phases are displaced by 120 electrical degrees from each other, and the rotor phase are also displaced by 120 electrical degrees from each other. The angle between the magnetic axes of stator phase winding, A, and rotor phase winding, a, is σ. The speed of the rotor is $w_r = d\sigma/dt$ and its direction is also shown in Figure 2.5, in the counter-clockwise direction.

The following assumptions are adopted for developing the ABC model [11]:

- The stator and rotor phases of the DFIG are supposed symmetrically distributed, which means that the resistances, magnetizing and leakage inductances for all three phases are equal.

- The produced magneto motive force is sinusoidally distributed around the circumference of the stator of the DFIG. Therefore, no harmonic components will be present.

- The air-gap is assumed constant, which means constant air-gap reluctance around the circumference of the mid-air-gap circle.

- Saturation of the mutual inductances is neglected.

- Skin effect in the stator and rotor phase winding conductors is neglected. When the frequency of the current increases, skin effect will firstly increase the reluctance of the leakage flux permeances of the DFIG, which will further increase the resistances and decrease the leakage inductances.

- Core losses are neglected, and only the power losses on the stator and rotor phase resistances are considered.

- Cross-saturation effect, that is, the coupling between two perpendicular axes, is neglected.

Consider phase A, this phase is signified by a coil as shown in Figure 2.5. The terminal voltage of phase A, v_A can be expressed based on Faraday's law as follows [127]:

$$v_A = r_A i_A + \frac{d}{dt}(\psi_A) \tag{2.7}$$

$$v_A = r_A i_A + \frac{d}{dt}\left(L_{AA}i_A + L_{AB}i_B + L_{AC}i_C + L_{Aa}i_a + L_{Ab}i_b + L_{Ac}i_c\right) \tag{2.8}$$

For phases B and C, similar expressions are written as follows:

$$v_B = r_B i_B + \frac{d}{dt}\left(L_{AB}i_A + L_{BB}i_B + L_{BC}i_C + L_{Ba}i_a + L_{Bb}i_b + L_{Bc}i_c\right) \tag{2.9}$$

$$v_C = r_C i_C + \frac{d}{dt}\left(L_{AC}i_A + L_{BC}i_B + L_{CC}i_C + L_{Ca}i_a + L_{Cb}i_b + L_{Cc}i_c\right) \tag{2.10}$$

For a symmetrical condition, the stator resistances can be expressed as follows:

$$r_A = r_B = r_C = r_S \tag{2.11}$$

Where r_S is resistance of a stator phase winding.

Similar expressions can be written for the coils representing phases a, b and c, on the rotor, and given as follows:

$$v_a = r_a i_a + \frac{d}{dt}\left(L_{Aa}i_A + L_{Ba}i_B + L_{Ca}i_C + L_{aa}i_a + L_{ab}i_b + L_{ac}i_c\right) \tag{2.12}$$

$$v_b = r_b i_b + \frac{d}{dt}\left(L_{Ab}i_A + L_{Bb}i_B + L_{Cb}i_C + L_{ab}i_a + L_{bb}i_b + L_{bc}i_c\right) \tag{2.13}$$

$$v_c = r_c i_c + \frac{d}{dt}\left(L_{Ac}i_A + L_{Bc}i_B + L_{Cc}i_C + L_{ac}i_a + L_{bc}i_b + L_{cc}i_c\right) \tag{2.14}$$

Again, the rotor resistances can be expressed as follows:

$$r_A = r_B = r_C = r_r \tag{2.15}$$

Where r_r is resistance of a rotor phase winding.

From the geometries shown in Figure 2.5, the inductance coefficients L_{AA}, L_{BB} and L_{CC}, are equal since the flux path for three phase windings, A, B and C, are identical. Also, these inductances are independent of the rotor position σ. Hence L_{AA}, L_{BB} and L_{CC}, can be expressed as follows:

$$L_{AA} = L_{BB} = L_{CC} = L_{SS} \tag{2.16}$$

Similarity, it can be seen from Figure 2.5 that the inductances L_{AB}, L_{BC} and L_{CA} are equal in magnitude, and that they are independent of the rotor position σ. Hence, these inductances can be expressed as follows:

$$L_{AB} = L_{BC} = L_{AC} = L_{SM} \tag{2.17}$$

Similarly, for the rotor inductance coefficients, $L_{aa}, L_{bb}, L_{cc}, L_{ab}, L_{bc}$ and L_{ac}, can be deduced that they are all independent of the rotor position, σ hence,

$$L_{aa} = L_{bb} = L_{cc} = L_{rr} \tag{2.18}$$

$$L_{ab} = L_{bc} = L_{ac} = L_{rm} \tag{2.19}$$

19

All other coefficients of inductance are dependent on the angular position of the rotor phase windings with respect to the stator phase windings. From the geometries shown in Figure 2.5, it can be easily deduced that all these coefficients vary correspondingly with the rotor angular position, σ with phase differences. The expressions for these inductances are written as follows:

$$L_{Aa} = L_{Bb} = L_{Cc} = L_{srm} \cos(\sigma) \tag{2.20}$$

$$L_{Ab} = L_{Bc} = L_{Ca} = L_{srm} \cos\left(\sigma + \frac{2\pi}{3}\right) \tag{2.21}$$

$$L_{Ac} = L_{Ba} = L_{Cb} = L_{srm} \cos\left(\sigma - \frac{2\pi}{3}\right) \tag{2.22}$$

where, L_{srm} is the maximum mutual-inductance between the stator phase windings and rotor phase windings, and σ is the angle between the a-axis on the rotor and the A-axis on the stator, which is equal to $\sigma = \sigma_0 + \int_0^t \omega_r(t)dt$.

2.6.2 DFIG Model Expressed in a DQO Synchronously Rotating Reference Frame

The DFIG model expressed in a synchronously rotating reference frame has the advantage that the time varying variables of the three-phase system, such as stator currents and voltages, rotor currents and voltages, become constants. This feature will be very useful in formulating and implementing any digital control systems. In this thesis, for control purposes, the DFIG model conveyed in a synchronously rotating reference frame will be chosen, and the deduction of the develop torque, active power and reactive power conveyed in a synchronously rotating reference frame will be given later in this section.

Instead of fixing the D-axis on the rotor or on the stator, the D-axis in the induction machine model expressed in a synchronously rotating reference frame will rotate at synchronous speed. Consider the schematic diagram of the ABC to DQO-dqo synchronously rotating reference frame transformation, which is shown in Figure 2.6.
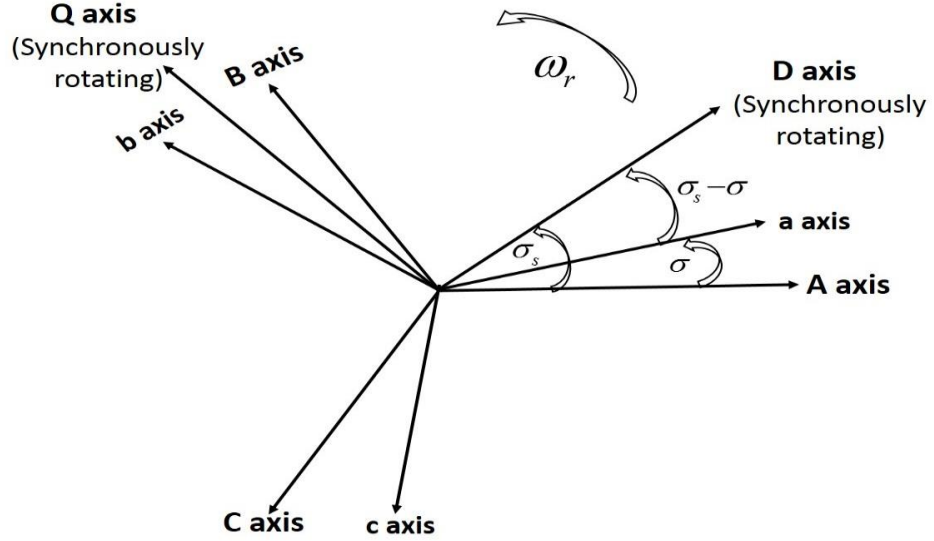
Figure 2.6 Schematic diagram of the ABC to DQO

Synchronously rotating reference frame transformation

Here, σ_s is the angle between the stator A-axis and the synchronously rotating D-axis,

and is equal to $\sigma_s = \sigma_{s0} + \int_0^t \omega_s(t)dt$, or $\sigma_s = \sigma_{s0} + \omega_s t$, for a fixed operation angular

speed/frequency.

Where, ω_s is the synchronous speed.

By using the same logic and steps of DQO-dqo models developed as in the two previous

cases, the stator and rotor transformation matrices, T_{sro} and T_{rro}, can be deduced as

follows:

$$T_{sro} = \frac{2}{3}\begin{bmatrix} \cos(\sigma) & \cos\left(\sigma - \frac{2\pi}{3}\right) & \cos\left(\sigma + \frac{2\pi}{3}\right) \\ -\sin(\sigma) & -\sin\left(\sigma - \frac{2\pi}{3}\right) & -\sin\left(\sigma + \frac{2\pi}{3}\right) \\ \frac{1}{2} & \frac{1}{2} & \frac{1}{2} \end{bmatrix} \tag{2.23}$$

$$T_{rro} = \frac{2}{3}\begin{bmatrix} 1 & -\frac{1}{2} & -\frac{1}{2} \\ 0 & \frac{\sqrt{3}}{2} & -\frac{\sqrt{3}}{2} \\ \frac{1}{2} & \frac{1}{2} & \frac{1}{2} \end{bmatrix} \tag{2.24}$$

When dq-frame delay by 90^0, the stator and rotor transformation matrices, T_{sro} and T_{rro}, can be deduced as follows:

$$T_{sro} = \frac{2}{3} \begin{bmatrix} \sin(\sigma) & \sin\left(\sigma - \frac{2\pi}{3}\right) & \sin\left(\sigma + \frac{2\pi}{3}\right) \\ \cos(\sigma) & \cos\left(\sigma - \frac{2\pi}{3}\right) & \cos\left(\sigma + \frac{2\pi}{3}\right) \\ \frac{1}{2} & \frac{1}{2} & \frac{1}{2} \end{bmatrix} \tag{2.25}$$

$$T_{rro} = \frac{2}{3} \begin{bmatrix} 0 & -\frac{\sqrt{3}}{2} & \frac{\sqrt{3}}{2} \\ 1 & -\frac{1}{2} & \frac{1}{2} \\ \frac{1}{2} & \frac{1}{2} & \frac{1}{2} \end{bmatrix} \tag{2.26}$$

2.7 Back-to-Back Voltage Source Converter (VSC) Models

PWM voltage source converters are commonly used in AC motor drives to produce sinusoidal AC output voltages whose magnitudes and frequency can both be controlled. Since in DFIG-based wind turbine-generator systems, a DFIG needs to be operated either in sub-synchronous speed mode or super-synchronous speed mode according to various wind speeds. Therefore, the back-to-back power converter configurations become necessary due to their bi-directional operation ability.

In order to achieve the above objectives, it would be necessary to study the back-to-back converter model. In this section, a grid-side converter which actually plays the same role as a PWM rectifier is considered for the modelling study. A three-phase PWM voltage source rectifier model is first established in a straightforward ABC reference frame, and the ABC model is transformed to a DQO synchronous reference frame to simplify the controller design.

2.7.1 Three Phase VSC Model Expressed in the ABC Reference Frame

The circuit of a three-phase PWM voltage source converter is shown in Figure 2.7 consists of six IGBTs with body diodes, three-phase AC input inductances and resistances, and a DC output capacitor.
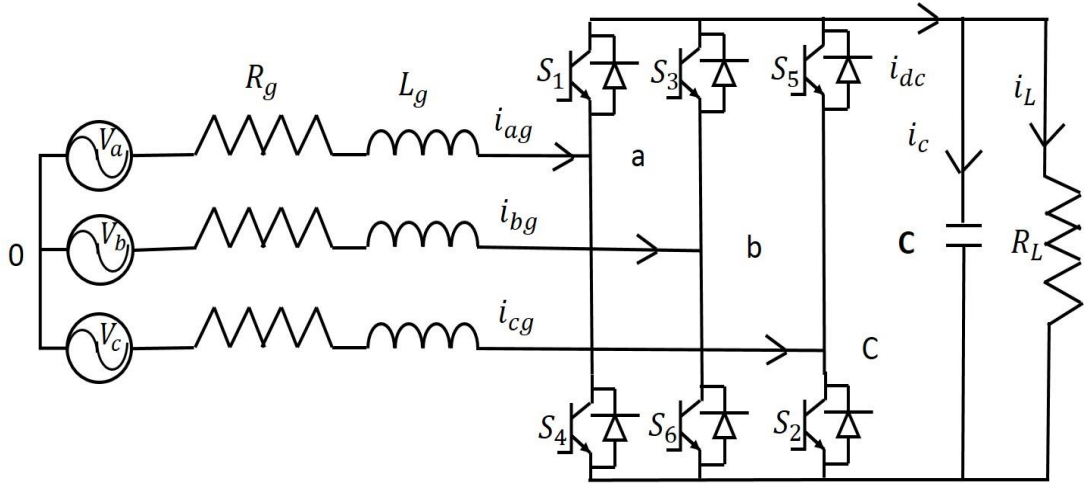
Figure 2.7 Configuration of a PWM voltage source rectifier

Here, $V_a(t)$, $V_b(t)$ and $V_c(t)$ are the three-phase voltage sources simulating an infinite-bus as a feed node in the power system, $R_g's$ are the AC side resistances, and $L_g's$ are the AC side inductances. Here, C, is the DC-link capacitor, R_L is the load resistance, while i_{ag}, i_{bg} and i_{cg} are the input currents of a three-phase PWM rectifier. Here also, i_{dc} is the DC-link current, i_L is the load current, and V_{dc} is the voltage across the capacitor.

The modelling and circuit analysis of the PWM rectifier is given next. First, let us define $S_k(K = a,b,c)$ as the switch function of phase, K. Based on the principle that any two switches in the same leg cannot be on at the same time, one can write the following definition [28]:

$$S_k = \begin{cases} 1 & upper \quad IGBT \quad on \\ 0 & upper \quad IGBT \quad off \end{cases} \tag{2.27}$$

Applying Kirchhoff's laws to the circuit of Figure 2.7, the instantaneous values of the currents can be obtained, and written as following:

$$\begin{cases} L_g \dfrac{di_{ag}}{dt} = V_a - R_g i_{ag} - V_{(a,0)} \\[2mm] L_g \dfrac{di_{bg}}{dt} = V_b - R_g i_{bg} - V_{(b,0)} \\[2mm] L_g \dfrac{di_{cg}}{dt} = V_c - R_g i_{cg} - V_{(c,0)} \end{cases} \tag{2.28}$$

23

Here $V_{(a,0)}$, $V_{(b,0)}$ and $V_{(c,0)}$, are the voltages from the ac side of the VSC to the power neutral point 0, and can be obtained by (2.29).

$$\begin{cases} V_{(a,0)} = V_{(a,N)} + V_{(N,0)} \\ V_{(b,0)} = V_{(b,N)} + V_{(N,0)} \\ V_{(c,0)} = V_{(c,N)} + V_{(N,0)} \end{cases} \tag{2.29}$$

Where $V_{(N,0)}$ is the voltage from point N to point 0. Here $V_{(a,N)}$, $V_{(b,N)}$ and $V_{(c,N)}$ are the voltages from the AC side of the PWM rectifier to point N.

For a balanced three-phase system, one can write:

$$V_{(a,0)} + V_{(b,0)} + V_{(c,0)} = 0 \tag{2.30}$$

Substituting from equation (2.29) into (2.30), the following equation can be deduced:

$$V_{(N,0)} = -\frac{V_{(a,N)} + V_{(b,N)} + V_{(c,N)}}{3} \tag{2.31}$$

Considering phase-a, when the upper switch is on and lower switch is off, $S_a = 1$ and $V_{(a,N)} = V_{dc}$. Similarity, when the upper switch is off and lower switch is on, $S_a = 0$ and $V_{(a,N)} = 0$. Therefore, based on the above characteristic, $V_{(a,N)} = V_{dc}.S_a$.

Therefore $\begin{cases} V_{(a,N)} = S_a V_{dc} \\ V_{(b,N)} = S_b V_{dc} \\ V_{(c,N)} = S_c V_{dc} \\ V_{(N,0)} = -\dfrac{1}{3}\left(S_a + S_b + S_c\right)V_{dc} \end{cases}$ \hfill (2.32)

Substituting from (2.29) and (2.32) into (2.28), the set of (2.33) derived as:

$$\begin{cases} L_g \dfrac{di_{ag}}{dt} = V_a - R_g i_{ag} - V_{dc}\left(S_a - \dfrac{1}{3}\sum_{k=a,b,c} S_k\right) \\ L_g \dfrac{di_{bg}}{dt} = V_b - R_g i_{bg} - V_{dc}\left(S_b - \dfrac{1}{3}\sum_{k=a,b,c} S_k\right) \\ L_g \dfrac{di_{cg}}{dt} = V_c - R_g i_{cg} - V_{dc}\left(S_c - \dfrac{1}{3}\sum_{k=a,b,c} S_k\right) \end{cases} \tag{2.33}$$

Under the assumption that the power switch resistances of a balanced three-phase system could be neglected, the power relationship between the dc side and ac side is given as follows:

$$\sum_{k=a,b,c} i_{kg}(t)V_{kN}(t) = i_{dc}(t)V_{dc} \tag{2.34}$$

By combining (2.32) with (2.33), the following (2.35) as:

$$i_{dc}(t) = i_{ag}(t)S_a + i_{bg}(t)S_b + i_{cg}(t)S_c \tag{2.35}$$

By applying Kirchhoff's laws to the positive node of the capacitor, given as:

$$\begin{cases} i_c = C\dfrac{dV_{dc}}{dt} \\ i_{dc} = i_c + i_L \\ i_{dc} = S_a i_{ag} + S_b i_{bg} + S_c i_{cg} \\ i_L = \dfrac{V_{dc}}{R_L} \end{cases} \tag{2.36}$$

(2.36) can also be expressed by a single equation, and given as follows [11]:

$$C\frac{dV_{dc}}{dt} = S_a i_{ag} + S_b i_{bg} + S_c i_{cg} - \frac{V_{dc}}{R_L} \tag{2.37}$$

For a balanced three-phase system

$$V_a + V_b + V_c = 0 \tag{2.38}$$

$$i_{ag} + i_{bg} + i_{cg} = 0 \tag{2.39}$$

Therefore, (2.33) along with (2.37) through (2.39) constitute the three-phase voltage source converter model obtained in the abc frame, and are rewritten as [12]:

$$\begin{cases} C\dfrac{dV_{dc}}{dt} = \sum_{k=a,b,c} S_k i_{kg} - i_L \\ L_g\dfrac{di_{kg}}{dt} + R_g i_{kg} = V_k - V_{dc}\left(S_k - \dfrac{1}{3}\sum_{j=a,b,c} S_j\right), k = a,b,c \\ \sum_{k=a,b,c} V_k = \sum_{k=a,b,c} i_{kg} = 0 \end{cases} \tag{2.40}$$

2.7.2 Modelling of Three Phase VSC Expressed in DQ Synchronous Reference Frame

Although the voltage source converter model expressed in the abc frame has straightforward meanings, all the components in the abc model are time variant, which will bring troubles and difficulties to controller designs. Hence, it is necessary to convert the abc model to a dq model which rotates at synchronous speed, so that the three-phase voltage inputs and the current components will be transformed to dc values.

Applying the transformation matrix (2.41) in (2.40) and eliminating the zero-sequence components due to a balanced three-phase system, the VSC model articulated in the dq synchronous reference frame can be deduced and given as in [13], [14]:

$$T_{dqo} = \frac{2}{3} \begin{bmatrix} \cos(\sigma) & \cos\left(\sigma - \frac{2\pi}{3}\right) & \cos\left(\sigma + \frac{2\pi}{3}\right) \\ -\sin(\sigma) & -\sin\left(\sigma - \frac{2\pi}{3}\right) & -\sin\left(\sigma + \frac{2\pi}{3}\right) \\ \frac{1}{2} & \frac{1}{2} & \frac{1}{2} \end{bmatrix} \tag{2.41}$$

$$\theta = \omega t$$

$$\begin{cases} C\dfrac{dV_{dc}}{dt} = \dfrac{3}{2}\left(i_{dg}S_d + i_{qg}S_q\right) - i_L \\[2mm] L_g \dfrac{di_{dg}}{dt} - wL_g i_{qg} + R_g i_{dg} = V_d - V_{d1} \\[2mm] L_g \dfrac{di_{qg}}{dt} + wL_g i_{dg} + R_g i_{qg} = V_q - V_{q1} \end{cases} \tag{2.42}$$

Where, $V_{d1} = V_{dc}S_d$ and $V_{q1} = V_{dc}S_q$.

The real and reactive power of a grid-side converter expressed in the dq synchronous reference frame are given as follows:

$$P_g = \frac{3}{2}\left(V_d i_{dg} + V_q i_{qg}\right) \tag{2.43}$$

$$Q_g = \frac{3}{2}\left(V_q i_{dg} - V_d i_{qg}\right) \tag{2.44}$$

2.7.3 PI Control Design of a Grid Side VSC

Aligning the reference frame along the d-axis, the q-axis of the grid voltage, V_q will be zero, while the d-axis of the grid voltage, V_d will be a constant.

From the above analysis and from (2.43) and (2.44), the real and reactive power of a grid-side converter under such reference frame will be proportional to the currents, i_{dg} and i_{qg}, respectively. The relationships are given as in [11]:

$$P_g = \frac{3}{2} V_d i_{dg} \tag{2.45}$$

$$Q_g = -\frac{3}{2} V_d i_{qg} \tag{2.46}$$

Since the objective is to yield an UPF looking from the grid-side, the reactive power should be zero, and thus the reference value for the q-axis current is zero. Hence, through controlling the d-axis and q-axis currents, the real and reactive power flow between the grid and the grid-side converter can be regulated.

From (2.42), the d and q axes equations have coupling components, $wL_g i_{qg}$ and $wL_g i_{dg}$. Therefore, a decoupled control scheme is recommended, and the corresponding control signals are given as follows [13], [9]

$$\begin{cases} V_{d1} = -R_g i_{dg} + wL_g i_{qg} + V_d + \Delta V_d \\ V_{q1} = -R_g i_{qg} - wL_g i_{dg} + V_q + \Delta V_q \end{cases} \tag{2.47}$$

The decoupled state equation is written as follows:

$$\begin{cases} L_g \dfrac{di_{dg}}{dt} + \Delta V_d = 0 \\ L_g \dfrac{di_{qg}}{dt} + \Delta V_q = 0 \end{cases} \tag{2.48}$$

The voltage error is produced by comparing the actual dc voltage with the reference dc voltage. The voltage error signal is processed through a PI controller to

keep constant dc voltage. In relates to the PI controller, a reference current signal i_{gd}^* is produced and q-axis current part i_{gq}^* is set as zero, to maintain UPF at the grid.

$$i_{gd}^* = \left(k_{p1} + \frac{k_{i1}}{s} \right)\left(V_{dc}^* - V_{dc} \right)$$
(2.49)

Now, the control signals for grid converter are obtained by comparing the reference grid currents i_{gd}^* and i_{qg}^* with the actual grid currents as,

$$\Delta V_d = \left(k_{p2} + \frac{k_{i2}}{s} \right)\left(i_{gd}^* - i_{gd} \right)$$
(2.50)

$$\Delta V_q = \left(k_{p3} + \frac{k_{i3}}{s} \right)\left(i_{gq}^* - i_{gq} \right)$$
(2.51)

Choosing the dc-link reference voltage from (2.52). [14]

$$V_{dc} \propto \frac{\sqrt{2}V_a}{m}$$
(2.52)

The modulation signal for phase-a can be derived as follows [15]:

$$V_{ma} = \frac{2V_{a1}V_T}{V_{dc}}$$
(2.53)
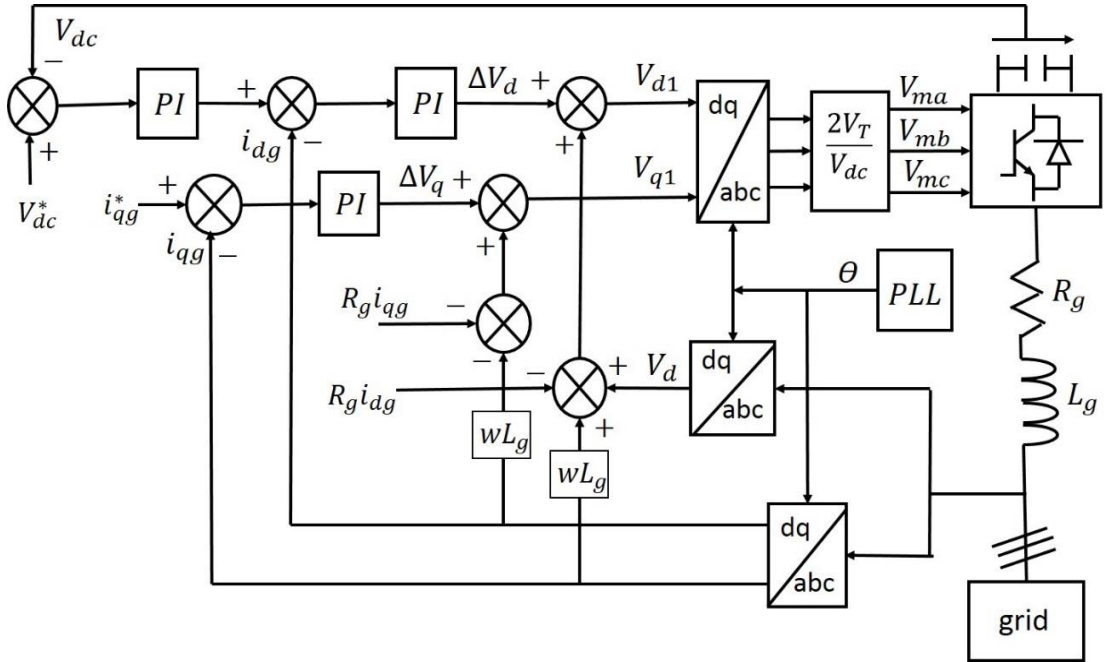
Figure 2.8 Grid side VSC control scheme

28

2.7.4   Results and Discussion

To confirm the efficiency of the given control scheme, the closed loop control system for a grid side VSC is simulated.

Fig.2.9 shows grid current is synchronized and for better visibility the time offset is set to 0.7 sec. so the control strategy is reasonable to apply for grid side converter based wind energy conversion system. Fig.2.10 shows the voltage across the capacitor is maintained constant at 800 V. The dc-link voltage response of the grid side VSC what the input voltages are, the grid side converter control scheme will try to keep constant dc voltage is shown in Fig.2.11. In Fig.2.12, the dc side active power is near 17 KW. To supply the dissipated energy of the resistor $R_L = 37.5\ \Omega$, the VSC needs to provide power flow near 17 KW to the dc bus. In Fig.2.13 the reactive power approximately zero and it ensures the UPF operation of the system. In dq synchronous reference frame, d-axis align with grid phase-a voltage i.e. d-axis voltage equals to the peak amplitude of grid phase-a voltage and q-axis voltage equals to zero are shown in Fig.2.14 and Fig.2.15.
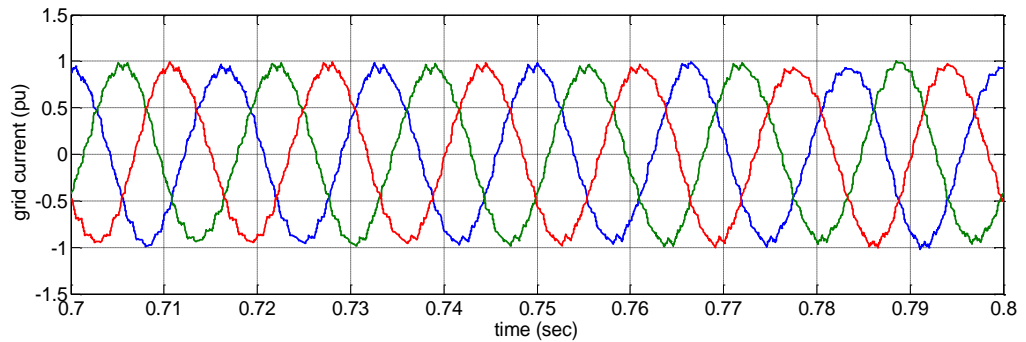
Fig.2.9   Grid current
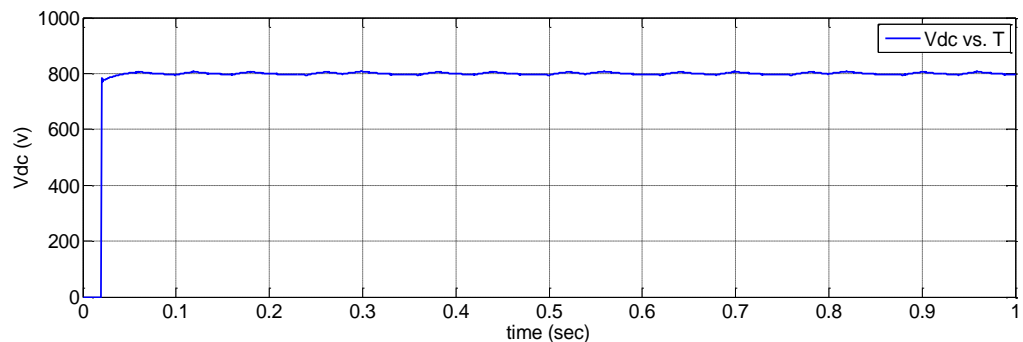
Fig.2.10   DC-link voltage
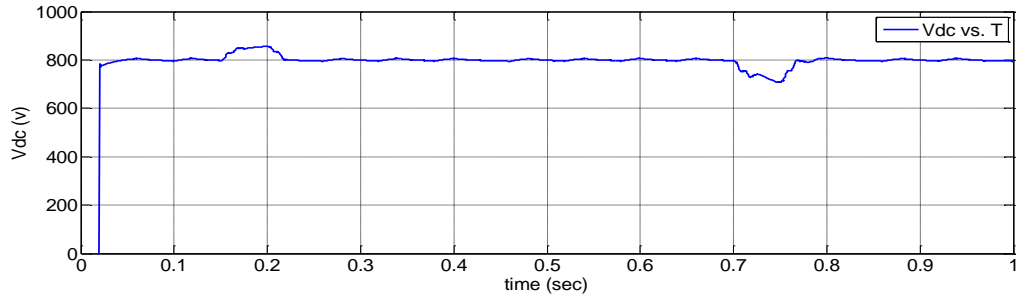
Fig.2.11   DC-link voltage with grid sag and swell
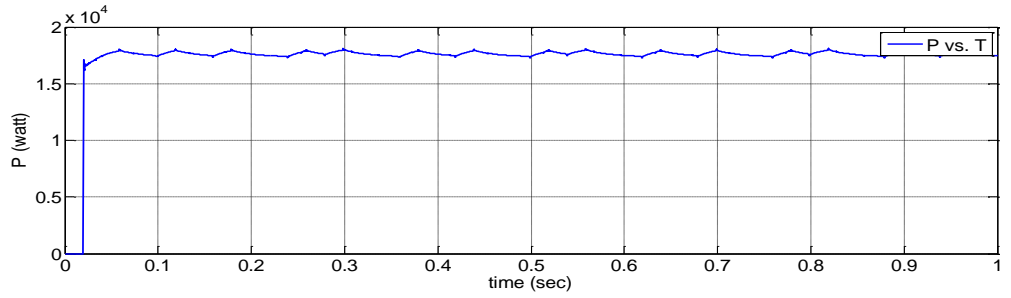
Fig.2.12   Active power of the grid
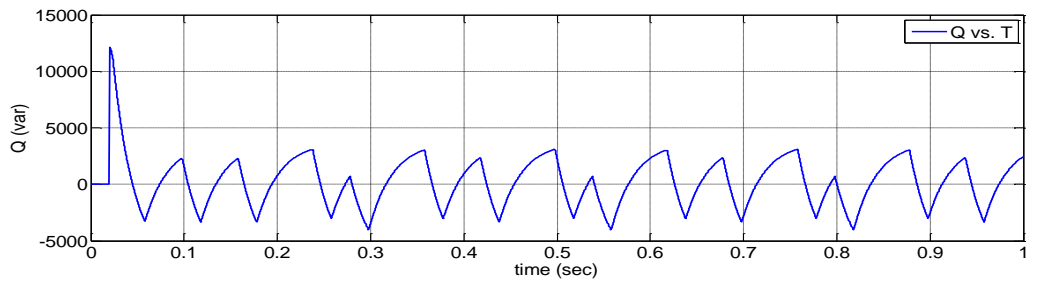
Fig.2.13   Reactive power of the grid
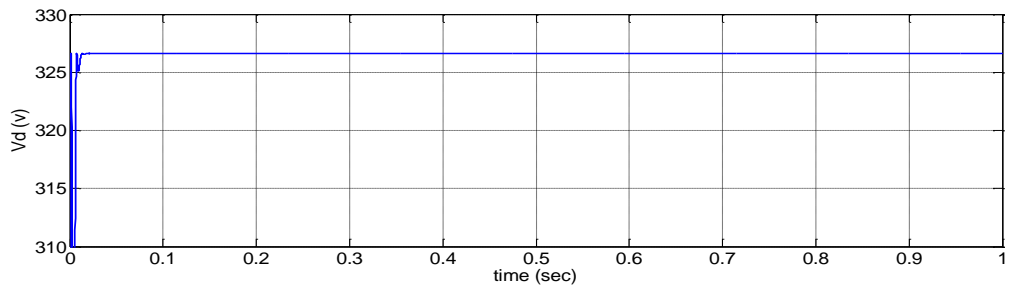
Fig.2.14   Direct-axis voltage of the grid
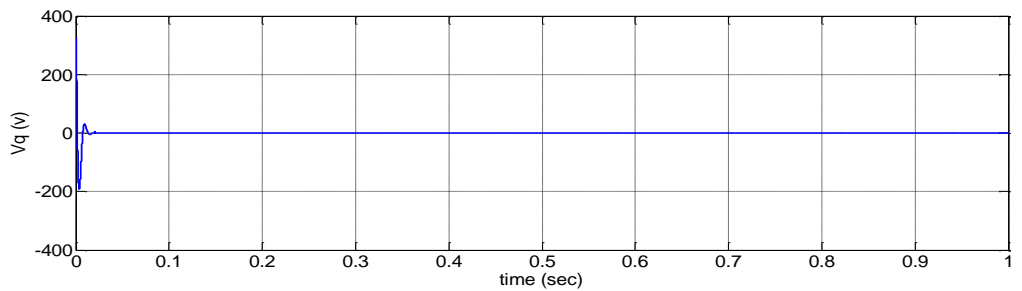
Fig.2.15   Quadrature-axis voltage of the grid

Chapter 3

Doubly Fed Induction Generator based Wind Energy Conversion System

3.1 Introduction

This chapter presents a detailed explanation about DFIG-based WECS. The overall components of DFIG-based WECS are discussed first. Its operation modes, modelling, control system design, and the detail explanations about each significant component are presented later.

Among different wind generation technologies available, variable-speed variable-pitch wind turbines utilizing DFIGs are the most popular in the wind power industry especially for multi-megawatt wind turbine generators [8].

3.2 Modelling of DFIG for WECS

The DFIG consists of stator and rotor windings which are constructed by three-phase insulated windings and is equipped with slip rings. The stator is connected to the grid through a three-phase transformer. By means of these components, the controlled rotor current can be either injected to or absorbed from the rotor windings.

The dynamics of the DFIG is using the qd-frame as given in (3.1)-(3.4) [54]:

$$V_{qs} = R_s I_{qs} + \omega_e \psi_{ds} + \frac{d}{dt}\psi_{qs} \tag{3.1}$$

$$V_{ds} = R_s I_{ds} - \omega_e \psi_{qs} + \frac{d}{dt}\psi_{ds} \tag{3.2}$$

$$V_{qr} = R_r I_{qr} + (\omega_e - \omega_r)\psi_{dr} + \frac{d}{dt}\psi_{qr} \tag{3.3}$$

$$V_{dr} = R_r I_{dr} + (\omega_e - \omega_r)\psi_{qr} + \frac{d}{dt}\psi_{dr} \tag{3.4}$$

The flux linkage equations are given as:

$$\psi_{qs} = L_s I_{qs} + L_m I_{qr} \tag{3.5}$$

$$\psi_{ds} = L_s I_{ds} + L_m I_{dr} \tag{3.6}$$

$$\psi_{qr} = L_m I_{qs} + L_r I_{qr} \tag{3.7}$$

$$\psi_{dr} = L_m I_{ds} + L_r I_{dr} \tag{3.8}$$

Where $L_s = L_{ls} + L_m$ and $L_r = L_{lr} + L_m$

Solving (3.5) - (3.8) in terms of current equations:

$$I_{qs} = \frac{1}{\sigma L_s}\psi_{qs} - \frac{L_m}{\sigma L_s L_r}\psi_{qr} \tag{3.9}$$

$$I_{ds} = \frac{1}{\sigma L_s}\psi_{ds} - \frac{L_m}{\sigma L_s L_r}\psi_{dr} \tag{3.10}$$

$$I_{qr} = -\frac{L_m}{\sigma L_s L_r}\psi_{qs} + \frac{1}{\sigma L_r}\psi_{qr} \tag{3.11}$$

$$I_{dr} = -\frac{L_m}{\sigma L_s L_r}\psi_{ds} + \frac{1}{\sigma L_r}\psi_{dr} \tag{3.12}$$

Where leakage coefficient $\sigma = \dfrac{L_s L_r - L_m^2}{L_s L_r}$

3.2.1 Dynamic Modelling of DFIG in State Space Equations

According to the basic definition, the space whose co-ordinate axes are the 'n' state variables with time as the implicit variable is called the state space. The variables of the state space (state variables) are elaborate to govern the state of the dynamic system. Basically these are the energy storing elements contained in the system like inductor and capacitor. The fundamental equation of the state space is given as:

$$\begin{cases} \dot{X}(t) = AX(t) + BU(t) \\ Y(t) = CX(t) + DU(t) \end{cases} \tag{3.13}$$

Equation (3.13) is for linear time invariant system, where A, B, C, and D are state, input, output and feed forward matrices, respectively, X is the state vector and Y is the output vector. Equation (3.14) is for linear time variant system, where A, B, C, and D are time dependent matrices.

$$\begin{cases} \dot{X}(t) = A(t)X(t) + B(t)U(t) \\ Y(t) = C(t)X(t) + D(t)U(t) \end{cases} \tag{3.14}$$

In the DFIG system, the state variables are normally currents or fluxes. In the following section, the state variables for the DFIG has been derived as flux linkages. Substituting (3.9) - (3.12) into (3.1) - (3.4) gives the DFIG dynamics in the state space form as:

$$\frac{d}{dt}\psi_{qs} = -\frac{R_s}{\sigma L_s}\psi_{qs} - \omega_e\psi_{ds} + \frac{R_s L_m}{\sigma L_s L_r}\psi_{qr} + V_{qs} \tag{3.15}$$

$$\frac{d}{dt}\psi_{ds} = \omega_e\psi_{qs} - \frac{R_s}{\sigma L_s}\psi_{ds} + \frac{R_s L_m}{\sigma L_s L_r}\psi_{dr} + V_{ds} \tag{3.16}$$

$$\frac{d}{dt}\psi_{qr} = \frac{R_r L_m}{\sigma L_s L_r}\psi_{qs} - (\omega_e - \omega_r)\psi_{dr} - \frac{R_r}{\sigma L_r}\psi_{qr} + V_{qr} \tag{3.17}$$

$$\frac{d}{dt}\psi_{dr} = \frac{R_r L_m}{\sigma L_s L_r}\psi_{ds} - \frac{R_r}{\sigma L_r}\psi_{dr} + (\omega_e - \omega_r)\psi_{qr} + V_{dr} \tag{3.18}$$

Equations (3.15) - (3.18) are written in state space matrix form as:

$$\begin{bmatrix} \dot{\psi}_{qs} \\ \dot{\psi}_{ds} \\ \dot{\psi}_{qr} \\ \dot{\psi}_{dr} \end{bmatrix} = \begin{bmatrix} -\dfrac{R_s}{\sigma L_s} & -\omega_e & \dfrac{R_s L_m}{\sigma L_s L_r} & 0 \\ \omega_e & -\dfrac{R_s}{\sigma L_s} & 0 & \dfrac{R_s L_m}{\sigma L_s L_r} \\ \dfrac{R_r L_m}{\sigma L_s L_r} & 0 & \dfrac{R_r}{\sigma L_r} & (\omega_e - \omega_r) \\ 0 & \dfrac{R_r L_m}{\sigma L_s L_r} & (\omega_e - \omega_r) & -\dfrac{R_r}{\sigma L_r} \end{bmatrix} \begin{bmatrix} \psi_{qs} \\ \psi_{ds} \\ \psi_{qr} \\ \psi_{dr} \end{bmatrix} + \begin{bmatrix} 1 & 0 & 0 & 0 \\ 0 & 1 & 0 & 0 \\ 0 & 0 & 1 & 0 \\ 0 & 0 & 0 & 1 \end{bmatrix} \begin{bmatrix} V_{qs} \\ V_{ds} \\ V_{qr} \\ V_{dr} \end{bmatrix} \tag{3.19}$$

3.2.2 Active Power, Reactive Power and Torque Calculation

All the equations above are induction motor equations. When the induction motor operates as a generator, current direction will be opposite. Assuming negligible power losses in stator and rotor resistances, the active and reactive power outputs from stator and rotor side are given as:

$$P_s = \frac{3}{2}\left[V_{qs}I_{qs} + V_{ds}I_{ds}\right] \tag{3.20}$$

$$Q_s = \frac{3}{2}\left[V_{qs}I_{ds} - V_{ds}I_{qs}\right] \tag{3.21}$$

$$P_r = \frac{3}{2}\left[V_{qr}I_{qr} + V_{dr}I_{dr}\right] \tag{3.22}$$

$$Q_r = \frac{3}{2}\left[V_{qr}I_{dr} - V_{dr}I_{qr}\right] \tag{3.23}$$

The total active and reactive power generated by DFIG is:

$$P_{Total} = P_s + P_r \tag{3.24}$$

$$Q_{Total} = Q_s + Q_r \tag{3.25}$$

If P_{Total} and/or Q_{Total} is positive, DFIG is supplying power to the power grid, else it is drawing power from the grid.

The rotor speed dynamics of the DFIG is given as:

$$\frac{d}{dt}\omega_r = \frac{P}{2J}\left(T_m - T_e - C_f\omega_r\right) \tag{3.26}$$

The electromagnetic torque generated by the machine which proposed in terms of flux linkages and currents as follows:

$$T_e = \frac{3}{2}\left[\psi_{qs}I_{ds} - \psi_{ds}I_{qs}\right] \tag{3.27}$$

Where positive Te means DFIG works as a generator and negative value as a motor [55].

3.3 Control of DFIG-based WECS

The DFIG control is completed by control of the variable frequency converter, which includes RSC control and GSC control. The objective of the RSC is to allow for decoupled controlling the active and reactive power. This facilitates high flexibility which enables the turbine to capture maximum energy from wind and to provide reactive power support to the grid. The objective of the GSC is to maintain constant voltage across the capacitor irrespective of the magnitude and direction of the rotor power.

3.3.1 Design of the RSC Controller

The control structure involves of inner loop and outer loop in which the inner loop regulates the d-axis and q-axis rotor components, i.e. I_{dr} and I_{qr} , independently and the outer loop regulates the stator real power and reactive power autonomously. The stator voltage orientation (SVO) control principle for a DFIG is described in [31], where the q-axis of the rotating reference frame is aligned to the stator voltage i.e. $V_{ds} = 0$ and $V_{qs} = V_s$. From (3.15) and (3.16), the stator side flux can be controlled using PI

controller. In this study, the q-axis flux is regulated to zero ($\psi_{qs} = 0$) and ($\psi_{ds} = \psi_s$) for the de-coupled control of real and reactive power as described below (where $p = \dfrac{d}{dt}$ throughout the thesis):

$$\begin{cases} p\psi_{qs} + \dfrac{R_s}{\sigma L_s}\psi_{qs} = -\omega_e\psi_{ds} + \dfrac{R_s L_m}{\sigma L_s L_r}\psi_{qr} + V_{qs} \\[2mm] \sigma_{\psi qs} = -\omega_e\psi_{ds} + \dfrac{R_s L_m}{\sigma L_s L_r}\psi_{qr} + V_{qs} \\[2mm] \psi_{ds}^* = \dfrac{1}{\omega_e}\left(\dfrac{R_s L_m}{\sigma L_s L_r}\psi_{qr} + V_{qs} - \sigma_{\psi qs}\right) \end{cases} \tag{3.28}$$

$$\begin{cases} p\psi_{ds} + \dfrac{R_s}{\sigma L_s}\psi_{ds} = \omega_e\psi_{qs} + \dfrac{R_s L_m}{\sigma L_s L_r}\psi_{dr} + V_{ds} \\[2mm] \sigma_{\psi ds} = \omega_e\psi_{qs} + \dfrac{R_s L_m}{\sigma L_s L_r}\psi_{dr} + V_{ds} \\[2mm] \psi_{qs}^* = \dfrac{1}{\omega_e}\left(\sigma_{\psi ds} - \dfrac{R_s L_m}{\sigma L_s L_r}\psi_{dr} - V_{ds}\right) \end{cases} \tag{3.29}$$

Where $\sigma_{\psi qs} = p\psi_{qs} + \dfrac{R_s}{\sigma L_s}\psi_{qs} = K_{P\psi s} + \dfrac{K_{I\psi s}}{p}\left(\psi_{qs}^* - \psi_{qs}\right)$ and

$\sigma_{\psi ds} = p\psi_{ds} + \dfrac{R_s}{\sigma L_s}\psi_{ds} = K_{P\psi s} + \dfrac{K_{I\psi s}}{p}\left(\psi_{ds}^* - \psi_{ds}\right)$ are the outputs from the PI controllers.

The PI parameters are determined by comparing with the Butterworth polynomial which is described in the below section, are given as:

$$K_{P\psi s} = \sqrt{2}\omega_0 - \dfrac{R}{\sigma L_s} \tag{3.30}$$

$$K_{I\psi s} = \omega_0^2 \tag{3.31}$$

Now, neglecting frictional losses in (3.26) gives:

$$p\omega_r = \dfrac{P}{2J}\left(T_m - T_e\right) \tag{3.32}$$

Where T_m is the mechanical torque and is given as:

$$T_m = K_{opt}V_w^2 \tag{3.33}$$

Where $K_{opt} = \dfrac{R}{2\lambda_{opt}} \rho A C_{P\_opt}$ =constant and if the wind speed (V_w) is more than the

rated speed, the T_m is given as:

$$T_m = \frac{P_{rated}}{\omega_{rated}} \tag{3.34}$$

Where P_{rated} is rated power of the wind turbine and ω_{rated} is the rated speed of the wind turbine.

Equation (3.28) can be re-written as:

$$\frac{2J}{P} p\omega_r = (T_m - T_e) = \sigma_{wr} = K_{wr}\left(\omega_r^* - \omega_r\right) \tag{3.35}$$

Where K_{wr} is the PI controller for rotor speed controller, given as:

$$K_{wr} = \left(K_{Pwr} + \frac{K_{Iwr}}{p}\right)$$

Then (3.35) will be:

$$\begin{cases} \dfrac{2J}{P} p\omega_r = \left(K_{Pwr} + \dfrac{K_{Iwr}}{p}\right)\omega_r^* - \left(K_{Pwr} + \dfrac{K_{Iwr}}{p}\right)\omega_r \\[4mm] \dfrac{\omega_r}{\omega_r^*} = \dfrac{\dfrac{P}{2J}\left(pK_{wr} + K_{Iwr}\right)}{p^2 + p\dfrac{PK_{wr}}{2J} + \dfrac{PK_{Iwr}}{2J}} \end{cases} \tag{3.36}$$

Substituting $\psi_{qs} = 0$ in (3.27) and (3.5) results in (3.37).

$$\begin{cases} T_e = \dfrac{3}{2}\psi_{ds}I_{qs} \\[4mm] I_{qs} = -\dfrac{L_m}{L_s}I_{qr} \end{cases} \tag{3.37}$$

A further substitution of (3.36) into (3.35) and in combination with (3.31) results in:

$$T_e = \frac{3}{2}\psi_{ds}\left(-\frac{L_m}{L_s}\right)I_{qr} \tag{3.38}$$

$$I_{qr} = (\sigma_{wr} - T_m)\frac{2}{3}\frac{L_s}{L_m\psi_{ds}} \tag{3.39}$$

Now, the stator active power is given as:

$$P_s = \frac{3}{2}\left(V_{qs}I_{qs} + V_{ds}I_{ds}\right) = -\frac{3}{2}\frac{L_m}{L_s}V_{qs}I_{qr} \tag{3.40}$$

Now, the stator supplied reactive power is given as:

$$Q_s = \frac{3}{2}\left(V_{qs}I_{ds} - V_{ds}I_{qs}\right) = \frac{3}{2}V_{qs}I_{ds} \tag{3.41}$$

Substituting V_{qs} in (3.39) gives:

$$Q_s = \frac{3}{2}\left(R_s I_{qs} + \omega_e \psi_{ds} + p\psi_{qs}\right)I_{ds} \tag{3.42}$$

Assuming constant stator flux, neglecting the stator resistance and substituting I_{ds} from (3.10) gives:

$$Q_s = \frac{3}{2}\frac{\omega_e}{\sigma L_s}\left(\psi_{ds}^2 - \frac{L_m}{L_r}\psi_{ds}\psi_{dr}\right) \tag{3.43}$$

Differentiating (3.41) w.r.t. time gives:

$$pQ_s = -\frac{3}{2}\frac{\omega_e}{\sigma L_s}\frac{L_m}{L_r}\psi_{ds}p\psi_{dr} \tag{3.44}$$

From (3.42) and (3.4) and solving ψ_{qr} in terms of I_{qr} gives (3.45)

$$\begin{cases} pQ_s = -\frac{3}{2}\frac{\omega_e}{\sigma L_s}\frac{L_m}{L_r}\psi_{ds}\left(V_{dr} - R_r I_{dr} + \left(\omega_e - \omega_r\right)\psi_{qr}\right) \\ pQ_s = -\frac{3}{2}\frac{\omega_e}{\sigma L_s}\frac{L_m}{L_r}\psi_{ds}\left(V_{dr} - R_r I_{dr} + \left(\omega_e - \omega_r\right)\sigma L_r I_{qr}\right) \\ \nabla pQ_s = \sigma_{Qs} = K_{Qs}\left(Q_s^* - Q_s\right) \end{cases} \tag{3.45}$$

Where $\nabla = \frac{2\sigma L_s L_r}{3\omega_e L_m}$ and K_{Qs} is the PI controller for stator side reactive power

controller, given as: $K_{Qs} = \left(K_{PQs} + \frac{K_{IQs}}{p}\right)$. So, (3.45) can be re-written as:

$$\nabla pQ_s = \left(K_{PQs} + \frac{K_{IQs}}{p}\right)Q_s^* - \left(K_{PQs} + \frac{K_{IQs}}{p}\right)Q_s \tag{3.46}$$

$$\frac{Q_s}{Q_s^*} = \frac{\frac{1}{\nabla}\left(pK_{PQs} + K_{IQs}\right)}{p^2 + p\frac{K_{PQs}}{\nabla} + \frac{K_{IQs}}{\nabla}} \tag{3.47}$$

From (3.44) and (3.45) gives:

$$I_{dr}^* = \frac{1}{R_r}\left(V_{dr} + \left(\omega_e - \omega_r\right)\sigma L_r I_{qr} + \frac{\sigma_{Qs}}{\psi_{ds}}\right) \tag{3.48}$$

From Equations (3.38) and (3.48) that, P_s and Q_s are proportional to I_{qr} and I_{dr}. The mutual coupling term $(\omega_e - \omega_r)\sigma L_r I_{qr}$ in (3.48) is very small so its effect is negligible. The rotor current can be regulated by means of rotor voltages.

The relation between rotor current and rotor voltage is obtained by substituting values of ψ_{dr} and ψ_{qr} from (3.7) and (3.8) in Equations (3.3) and (3.4), respectively, and further simplification yields:

$$V_{qr} = R_r I_{qr} + \sigma L_r p I_{qr} + \omega_{sl}\left(\frac{L_m}{L_s}\psi_{ds} + \sigma L_r I_{dr}\right) \tag{3.49}$$

$$V_{dr} = R_r I_{dr} + \sigma L_r p I_{dr} - \omega_{sl}\sigma L_r I_{qr} \tag{3.50}$$

Where $\omega_{sl} = (\omega_e - \omega_r)$ and $\sigma = 1 - \dfrac{L_m^2}{L_s L_r}$

In the Equations (3.49) and (3.50), there is the term including I_{dr} in the q-axis equation and there is the term including I_{qr} in the d-axis equation. So these two equations are coupled and the traditional linear controllers cannot be used. However, through the exact linearization method, these equations can be linearized by putting the terms other than the currents control to one side.

$$R_r I_{qr} + \sigma L_r p I_{qr} = V_{qr} - \omega_{sl}\left(\frac{L_m}{L_s}\psi_{ds} + \sigma L_r I_{dr}\right) \tag{3.51}$$

$$R_r I_{dr} + \sigma L_r p I_{dr} = V_{dr} + \omega_{sl}\left(\sigma L_r I_{qr}\right) \tag{3.52}$$

Then the currents can be regulated by linear controllers as shown in Figure 3.15, where:

$$\sigma_{qr} = R_r I_{qr} + \sigma L_r p I_{qr} \tag{3.53}$$

$$\sigma_{dr} = R_r I_{dr} + \sigma L_r p I_{dr} \tag{3.54}$$

The idea behind this is to use the linear controllers that include integrations to calculate the derivative terms. And the nonlinear equations become linear when all the nonlinear terms are moved to the other side of the equations. Then the q and d-axis voltages are calculated as shown in Figure 3.15.

$$V_{qr}^* = \sigma_{qr} + \omega_{sl}\left(\frac{L_m}{L_s}\psi_{ds} + \sigma L_r I_{dr}\right) \tag{3.55}$$

$$V_{dr}^* = \sigma_{dr} - \omega_{sl}\left(\sigma L_r I_{qr}\right) \tag{3.56}$$

Using the inner current control loop has a significant advantage for the protection of the DFIG. It can naturally protect the system from over-current since current limiters can be easily inserted in the control scheme shown in Figure 3.15.

Since the general PI controllers are widely used and proved to be effective, they are also applied in the following analysis [63]. For I_{qr} current control loop from (3.51):

$$V_{qr}^{'} = R_r I_{qr} + \sigma L_r p I_{qr} = (R_r + p\sigma L_r) I_{qr} \tag{3.57}$$

$$V_{qr}^{'} = \left(K_{qp} + \frac{K_{qi}}{p} \right)(I_{qr}^{*} - I_{qr}) \tag{3.58}$$

$$(R_r + p\sigma L_r) I_{qr} = \left(K_{qp} + \frac{K_{qi}}{p} \right) I_{qr}^{*} - \left(K_{qp} + \frac{K_{qi}}{p} \right) I_{qr} \tag{3.59}$$

Similarly, for I_{dr} current control loop from (3.52):

$$V_{dr}^{'} = R_r I_{dr} + \sigma L_r p I_{dr} = (R_r + p\sigma L_r) I_{dr} \tag{3.60}$$

$$V_{dr}^{'} = \left(K_{qp} + \frac{K_{qi}}{p} \right)(I_{dr}^{*} - I_{dr}) \tag{3.61}$$

$$(R_r + p\sigma L_r) I_{dr} = \left(K_{qp} + \frac{K_{qi}}{p} \right) I_{dr}^{*} - \left(K_{qp} + \frac{K_{qi}}{p} \right) I_{dr} \tag{3.62}$$

Then the transfer functions between the reference and actual currents are changed to the following:

$$\frac{I_{qr}}{I_{qr}^{*}} = \frac{pK_{qp} + K_{qi}}{p^2 \sigma L_r + p(R_r + K_{qp}) + K_{qi}} = \frac{\frac{1}{\sigma L_r}(pK_{qp} + K_{qi})}{p^2 + p\frac{1}{\sigma L_r}(R_r + K_{qp}) + \frac{1}{\sigma L_r}K_{qi}} \tag{3.63}$$

$$\frac{I_{dr}}{I_{dr}^{*}} = \frac{pK_{dp} + K_{di}}{p^2 \sigma L_r + p(R_r + K_{dp}) + K_{di}} = \frac{\frac{1}{\sigma L_r}(pK_{dp} + K_{di})}{p^2 + p\frac{1}{\sigma L_r}(R_r + K_{dp}) + \frac{1}{\sigma L_r}K_{di}} \tag{3.64}$$

Choosing the appropriate control parameters is very important to gain good performance although the whole system might be able to work for a wide range of parameters. Many researchers select the gains based on the experience or just by trial and error. This is not good especially when the control system is designed for a new system. The most important objective is to maintain the system stability by selecting appropriate control parameters. And then those parameters can be tuned up corresponding to the specified performance requirement. There are some methods that

can be used to determine the system parameters that can keep the whole system in the stable region.

One of the methods is by using Butterworth polynomial to optimize the closed-loop Eigen value locations [63]. The Butterworth technique traces the Eigen values homogenously in the left-half s-plane on a circle with radius ω_0 , with its centre at the origin as shown in Figure 3.1.

The transfer function of a Butterworth polynomial of second order denominator is given as:

$$p^2 + \sqrt{2}\omega_0 p + \omega_0^2 = 0 \tag{3.65}$$

The PI parameters are determined by comparing the coefficients in (3.79) with the denominators of the corresponding transfer functions and then choosing appropriate ω_0

$$K_{qp} = K_{dp} = \sqrt{2}\omega_0 \sigma L_r - R_r \tag{3.66}$$

$$K_{qi} = K_{di} = \sigma L_r \omega_0^2 \tag{3.67}$$

Here ω_0 is the bandwidth of the current controller, which depends upon the design value. The RSC control scheme is shown in Figure 3.2.
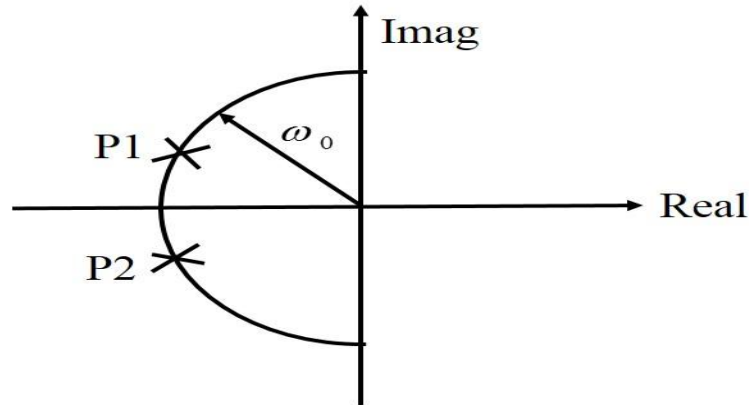
Figure 3.1 Location of poles for second order Butterworth polynomial

Figure 3.2 RSC control scheme

$$V_{dr}^{comp} = -\omega_{sl} \sigma L_r I_{qr} \text{ and } V_{qr}^{comp} = \omega_{sl}\left(\frac{L_m}{L_s}\psi_{ds} + \sigma L_r I_{dr}\right)$$

Similarly, comparing denominator of (3.33) with Butterworth second order

polynomial, i.e. $p^2 + \sqrt{2}\omega_{0wr}p + \omega_{0wr}^2$, PI controller gains are obtained as:

$$K_{Pwr} = \sqrt{2}\omega_{0wr}\frac{2J}{P} \tag{3.68}$$

$$K_{Iwr} = \omega_{0wr}^2\frac{2J}{P} \tag{3.69}$$

Where ω_{0wr} is the bandwidth frequency of the speed controller.

Similarly, comparing denominator of (3.47) with Butterworth second order

polynomial, i.e. $p^2 + \sqrt{2}\omega_{Qs}p + \omega_{Qs}^2$, PI controller gains are obtained as:

$$K_{PQs} = \sqrt{2}\omega_{0Qs}\nabla \tag{3.70}$$

$$K_{IQs} = \nabla\omega_{Qs}^2 \tag{3.71}$$

3.3.2 Design of the GSC Controller

The control mechanism of GSC which controls the voltage across the capacitor and reactive power exchange between the converter and grid is V_{dc} reached by controlling the current shown in Figure 3.3.

Now, DC voltage dynamics in DC-link is given by:

$$CpV_{dc} = \frac{3}{4}\left(M_{qr}I_{qr} + M_{dr}I_{dr}\right) + \frac{3}{4}\left(M_{df}I_{df} + M_{qf}I_{qf}\right) \qquad (3.72)$$

Where C is the capacitance, M_{dr} and M_{qr} are q and d-axis modulation indexes of RSC and M_{df}, M_{qf} are q and d-axis modulation indexes of GSC, respectively.

Hence, (3.72) can be re-written as (3.73) which can be solved to get I_{qf}.

$$CpV_{dc} = \frac{3}{4}\left(M_{qr}I_{qr} + M_{dr}I_{dr}\right) + \frac{3}{4}\left(M_{df}I_{df} + M_{qf}I_{qf}\right) = \sigma_{dc} \qquad (3.73)$$

Equation (3.73) can be re-written as:

$$CpV_{dc} = \sigma_{dc} = K_{dc}\left(V_{dc}^* - V_{dc}\right) \qquad (3.74$$

Where K_{dc} is the PI controller for DC-voltage control given as: $K_{dc} = \left(K_{Pdc} + \dfrac{K_{Idc}}{p}\right)$.

Then (3.74) will be:

$$CpV_{dc} = \left(K_{Pdc} + \frac{K_{Idc}}{p}\right)V_{dc}^* - \left(K_{Pdc} + \frac{K_{Idc}}{p}\right)V_{dc} \qquad (3.75)$$

$$\frac{V_{dc}}{V_{dc}^*} = \frac{\dfrac{1}{C_{dc}}\left(pK_{Pdc} + K_{Idc}\right)}{p^2 + p\dfrac{K_{Pdc}}{C_{dc}} + \dfrac{K_{Idc}}{C_{dc}}} \qquad (3.76)$$

Figure 3.3 Block diagram of GSC control system

Comparing denominator of (3.76) with Butterworth second order polynomial, i.e.

$p^2 + \sqrt{2}\omega_{0dc}p + \omega_{0dc}^2$, PI controller gains are obtained as:

$$K_{Pdc} = \sqrt{2}\omega_{0dc}C_{dc} \tag{3.77}$$

$$K_{Idc} = C_{dc}\omega_{0dc}^2 \tag{3.78}$$

Where ω_{0dc} is the bandwidth frequency of the DC-voltage controller. From (3.73):

$$I_{qf}^* = \frac{4}{3}\frac{1}{M_{qf}}\left(\sigma_{dc} - \frac{3}{4}\left(M_{qr}I_{qr} + M_{dr}I_{dr}\right)\right) - \frac{M_{df}}{M_{qf}}I_{df} \tag{3.79}$$

Using KVL across the RL filter gives:

$$V_{qf} = R_f I_{qf} + L_f pI_{qf} + \omega_e L_f I_{df} + \frac{V_{qs}}{N} = M_{qf}\frac{V_{dc}}{2} \tag{3.80}$$

$$V_{df} = R_f I_{df} + L_f pI_{df} - \omega_e L_f I_{qf} = M_{df}\frac{V_{dc}}{2} \tag{3.81}$$

Since the q-axis of the rotating reference frame is aligned to the stator voltage i.e.

$V_{ds} = 0$ and as $V_{qs} = V_s$. So, the GSC supplied reactive power to the grid is controlled

using d-axis current.

$$Q_f = \frac{3}{2N}V_s I_{df} \tag{3.82}$$

Where N is the transformer turns ratio connected between GSC and stator.

$$pQ_f = \frac{3V_s}{2N} pI_{df} \tag{3.83}$$

Substituting (3.81) in (3.83) gives:

$$pQ_f = \frac{3V_s}{2N} \frac{1}{L_f} \left(V_{df} - R_f I_{df} + \omega_e L_f I_{qf} \right) \tag{3.84}$$

$$\Gamma pQ_f = \left(V_{df} - R_f I_{df} + \omega_e L_f I_{qf} \right) = \sigma_{Qf} \tag{3.85}$$

Where $\Gamma = \dfrac{2NL_f}{3V_s}$

$$\Gamma pQ_f = \sigma_{Qf} = K_{Qf} \left(Q_f^* - Q_f \right) \tag{3.86}$$

Where K_{Qf} is the PI controller for reactive power supplied by GSC given as:

$$K_{Qf} = K_{PQf} + \frac{K_{IQf}}{p}.$$

Then (3.86) will be:

$$\Gamma pQ_f = \left(K_{PQf} + \frac{K_{IQf}}{p} \right) Q_f^* - \left(K_{PQf} + \frac{K_{IQf}}{p} \right) Q_f \tag{3.87}$$

$$\frac{Q_f}{Q_f^*} = \frac{\dfrac{1}{\Gamma} \left(pK_{PQf} + K_{IQf} \right)}{p^2 + p\dfrac{K_{PQf}}{\Gamma} + \dfrac{K_{IQf}}{\Gamma}} \tag{3.88}$$

Comparing denominator of (3.88) with Butterworth second order polynomial, i.e.

$p^2 + \sqrt{2}\omega_{0Qf} p + \omega_{0Qf}^2$, PI controller gains are obtained as:

$$K_{PQf} = \sqrt{2}\omega_{0Qf}\Gamma \tag{3.89}$$

$$K_{IQf} = \Gamma \omega_{0Qf}^2 \tag{3.90}$$

Where ω_{0Qf} is the bandwidth frequency of the reactive power controller. From (3.85).

$$I_{df}^* = \frac{1}{R_f} \left(V_{df} + \omega_e L_f I_{qf} - \sigma_{Qf} \right) \tag{3.91}$$

Equations (3.80) and (3.81) give the inner current control loop for the GSC control.

Inner current control:

If we assume:

$$R_f I_{qf} + L_f pI_{qf} = K_{qf} \left(I_{qf}^* - I_{qf} \right) = \sigma_{qf} \tag{3.92}$$

$$R_f I_{df} + L_f pI_{df} = K_{qf} \left(I_{df}^* - I_{df} \right) = \sigma_{df} \tag{3.93}$$

Then, (3.80) and (3.81) can be written as:

$$M_{qf} = \left(\sigma_{qf} + \omega_e L_f I_{df} + \frac{V_{qs}}{N} \right) \frac{2}{V_{dc}}$$
(3.94)

$$M_{df} = \left(\sigma_{df} - \omega_e L_f I_{qf} \right) \frac{2}{V_{dc}}$$
(3.95)

Equations (3.94) and (3.95) give modulation indexes which are the output of the converter. K_{qf} and K_{df} are PI current controllers for q and d-axis currents, respectively

and $K_{qf} = K_{df} = K_{P1} + \dfrac{K_{I1}}{p}$

Then, (3.92) can be re-written as:

$$\frac{I_{qf}}{I_{qf}^*} = \frac{\dfrac{1}{L_f}\left(pK_{P1} + K_{I1}\right)}{p^2 + p\dfrac{1}{L_f}\left(R_f + K_{P1}\right) + \dfrac{1}{L_f}K_{I1}}$$
(3.96)

Comparing denominator of (3.96) with the Butterworth second order polynomial gives:

$$K_{P1} = \sqrt{2}\omega_{0C} L_f - R_f$$
(3.97)

$$K_{I1} = L_f \omega_{0C}^2$$
(3.98)

3.3.3 Transfer Function of RSC and GSC Controllers

In the above mentioned controller design for RSC and GSC, each controllers are designed separately and finally combined together. This procedure is only valid when the controlled variables are independent of each other, i.e. they should be mutually decoupled. To check whether they are independent of each other or not, or if there should be any conditions to be fulfilled for the decoupled control of those two regulators, the RSC and GSC transfer functions are derived in this section. The conclusion is made at the end of this section.

From the flux control:

$$\begin{cases} \sigma_{\psi qs} = -\omega_e \psi_{ds} + \dfrac{R_s L_m}{\sigma L_s L_r} \psi_{qr} + V_{qs} \\[4mm] \sigma_{\psi qs} = -\omega_e \psi_{ds} + \dfrac{R_s L_m}{\sigma L_s L_r} \left(\sigma L_r I_{qr} + \dfrac{L_m}{L_s} \psi_{qs} \right) + V_{qs} \\[4mm] \sigma_{\psi qs} = -\omega_e \psi_{ds} + \dfrac{R_s L_m}{L_s} I_{qr} + \dfrac{R_s L_m^2}{\sigma L_s^2 L_r} \psi_{qs} + V_{qs} \\[4mm] K_{\psi s} \left(\psi_{qs}^* - \psi_{qs} \right) = -\omega_e \psi_{ds} + R_s \left(\dfrac{p8J\omega_r - 4PT_m}{3P^2 \psi_{ds}} \right) + \dfrac{R_s L_m^2}{\sigma L_s^2 L_r} \psi_{qs} + V_{qs} \end{cases} \tag{3.99}$$

$$\psi_{qs} = \frac{\sigma L_s^2 L_r \left(3P^2 K_{\psi s} \psi_{qs}^* + 3P^2 \psi_{ds} - 3P^2 V_{qs} \right)}{3R_s L_m^2 P^2 + 3P^2 \sigma L_s^2 L_r K_{\psi s}} - \frac{\sigma L_s^2 L_r R_s \left(p8J\omega_r - 4PT_m \right)}{\psi_{ds} \left(3R_s L_m^2 P^2 + 3P^2 \sigma L_s^2 L_r K_{\psi s} \right)} \tag{3.100}$$

Similarly,

$$\begin{cases} \sigma_{\psi ds} = \omega_e \psi_{qs} + \dfrac{R_s L_m}{\sigma L_s L_r} \psi_{dr} + V_{ds} \\[4mm] \sigma_{\psi ds} = \omega_e \psi_{qs} + \dfrac{R_s L_m}{\sigma L_s L_r} \left(\sigma L_r I_{dr} + \dfrac{L_m}{L_s} \psi_{ds} \right) + V_{ds} \\[4mm] \sigma_{\psi ds} = \omega_e \psi_{qs} + \dfrac{R_s L_m}{L_s} I_{dr} + \dfrac{R_s L_m^2}{\sigma L_s^2} \psi_{ds} + V_{ds} \\[4mm] K_{\psi s} \left(\psi_{ds}^* - \psi_{ds} \right) = \omega_e \psi_{qs} + \dfrac{R_s L_m^2}{\sigma L_s^2} \psi_{ds} - \dfrac{2R_s}{3} \dfrac{Q_s}{\omega_e \psi_{ds}} + V_{ds} \end{cases} \tag{3.101}$$

$$\psi_{ds} = \frac{K_{\psi s} \psi_{ds}^* - \omega_e \psi_{qs} + \dfrac{2R_s}{3} \dfrac{Q_s}{\omega_e \psi_{ds}} - V_{ds}}{\left(K_{\psi s} + \dfrac{R_s L_m^2}{\sigma L_s^2} \right)} \tag{3.102}$$

From (3.100) and (3.102), it is clear that the relations between control variable (ψ_{ds}, ψ_{qs}) and reference variable (ψ_{ds}^*, ψ_{qs}^*) are non-linear. Hence, transfer function cannot be obtained. Therefore, in the later part of the transfer function derivation, the stator fluxes are assumed constant as a result the relationship between control variables and reference variable is linear.

In the RSC, from (3.31):

$$\sigma_{wr} = K_{wr} \left(\omega_r^* - \omega_r \right) = \left(T_m - T_e \right) \tag{3.103}$$

$$\sigma_{wr} = T_m + \frac{3P}{4} \frac{\hat{L}_m}{\hat{L}_s} \psi_{ds} I_{qr}^* \tag{3.104}$$

$$I_{qr}^* = \left(\sigma_{wr} - T_m\right) \frac{4\hat{L}_s}{3P\hat{L}_m \psi_{ds}} \tag{3.105}$$

Where ($\wedge$) shows the measured value. Similarly, from (3.45):

$$\sigma_{Qs} = K_{Qs}\left(Q_s^* - Q_s\right) = \psi_{ds}\left(V_{dr} - \hat{R}_r I_{dr} + \hat{\omega}_{sl} \hat{\sigma} \hat{L}_r I_{qr}\right) \tag{3.106}$$

$$\sigma_{Qs} = \psi_{ds}\left(\hat{R}_r I_{dr} + p\hat{\sigma}\hat{L}_r I_{dr} - \hat{\omega}_{sl} \hat{\sigma} \hat{L}_r I_{qr} - \hat{R}_r I_{dr} + \hat{\omega}_{sl} \hat{\sigma} \hat{L}_r I_{qr}\right) \tag{3.107}$$

$$I_{dr}^* = \frac{\sigma_{Qs}}{p\hat{\sigma}\hat{L}_r \psi_{ds}} \tag{3.108}$$

From (3.105) and (3.108):

$$\begin{bmatrix} I_{qr}^* \\ I_{dr}^* \end{bmatrix} = \underbrace{\begin{bmatrix} \dfrac{4\hat{L}_s}{3P\hat{L}_m \psi_{ds}} & 0 \\ 0 & \dfrac{1}{p\psi_{ds} \hat{\sigma} \hat{L}_r} \end{bmatrix}}_{C} \begin{bmatrix} \sigma_{wr} \\ \sigma_{Qs} \end{bmatrix} + \underbrace{\begin{bmatrix} -\dfrac{4\hat{L}_s T_m}{3P\hat{L}_m \psi_{ds}} \\ 0 \end{bmatrix}}_{D} \tag{3.109}$$

From (3.28):

$$p\omega_r = \frac{P}{2J}\left(T_m - T_e\right) \tag{3.110}$$

$$p\omega_r = \frac{P}{2J}\left(T_m + \frac{3P}{4}\frac{L_m}{L_s}\psi_{ds}I_{qr}\right) \tag{3.111}$$

$$I_{qr} = \frac{p8J}{3P^2}\frac{L_s\omega_r}{L_m\psi_{ds}} - \frac{4T_m L_s}{3PL_m\psi_{ds}} \tag{3.112}$$

From (3.44):

$$pQ_s = -\frac{3}{2}\frac{\omega_e}{\sigma L_s}\frac{L_m}{L_r}\psi_{ds}\left(V_{dr} - R_r I_{dr} + \omega_{sl}\sigma L_r I_{qr}\right) \tag{3.113}$$

$$pQ_s = -\frac{3}{2}\frac{\omega_e}{\sigma L_s}\frac{L_m}{L_r}\psi_{ds}\left(R_r I_{dr} + p\sigma L_r I_{dr} - \omega_{sl}\sigma L_r I_{qr} - R_r I_{dr} + \omega_{sl}\sigma L_r I_{qr}\right) \tag{3.114}$$

$$I_{dr} = -\frac{2Q_s L_s}{3\omega_e L_m\psi_{ds}} \tag{3.115}$$

$$
\begin{bmatrix} I_{qr} \\ I_{dr} \end{bmatrix} = \underbrace{\begin{bmatrix} \dfrac{p8JL_s}{3PL_m\psi_{ds}} & 0 \\ 0 & -\dfrac{2L_s}{3\omega_e L_m\psi_{ds}} \end{bmatrix}}_{E} \begin{bmatrix} \omega_r \\ Q_s \end{bmatrix} + \underbrace{\begin{bmatrix} -\dfrac{4L_s T_m}{3PL_m\psi_{ds}} \\ 0 \end{bmatrix}}_{D}
\tag{3.116}
$$

From (3.59):

$$
\left(\hat{R}_r + p\,\hat{\sigma}\,\hat{L}_r \right) I_{qr} = K_{iqr} I_{qr}^* - K_{iqr} I_{qr}
\tag{3.117}
$$

From (3.62):

$$
\left(\hat{R}_r + p\,\hat{\sigma}\,\hat{L}_r \right) I_{dr} = K_{idr} I_{dr}^* - K_{idr} I_{dr}
\tag{3.118}
$$

Combining (3.117) and (3.118):

$$
\begin{bmatrix} I_{qr}^* \\ I_{dr}^* \end{bmatrix} = \underbrace{\begin{bmatrix} \dfrac{\hat{R}_r + p\,\hat{\sigma}\,\hat{L}_r + K_{iqr}}{K_{iqr}} & 0 \\ 0 & \dfrac{\hat{R}_r + p\,\hat{\sigma}\,\hat{L}_r + K_{idr}}{K_{idr}} \end{bmatrix}}_{K} \begin{bmatrix} I_{qr} \\ I_{dr} \end{bmatrix}
\tag{3.119}
$$

Substituting (3.109) and (3.116) in (3.119) gives:

$$
C \begin{bmatrix} \sigma_{wr} \\ \sigma_{Qs} \end{bmatrix} + D = KE \begin{bmatrix} \omega_r \\ Q_s \end{bmatrix} + KD
\tag{3.120}
$$

$$
\begin{bmatrix} \dfrac{4\hat{L}_s}{3P\hat{L}_m\psi_{ds}} & 0 \\ 0 & \dfrac{1}{p\psi_{ds}\,\hat{\sigma}\,\hat{L}_r} \end{bmatrix} \begin{bmatrix} K_{wr}\left(\omega_r^* - \omega_r\right) \\ K_{Qs}\left(Q_s^* - Q_s\right) \end{bmatrix} + \begin{bmatrix} -\dfrac{4\hat{L}_s T_m}{3P\hat{L}_m\psi_{ds}} \\ 0 \end{bmatrix}
$$

$$
= \begin{bmatrix} \dfrac{\hat{R}_r + p\,\hat{\sigma}\,\hat{L}_r + K_{iqr}}{K_{iqr}} \dfrac{p8JL_s}{3PL_m\psi_{ds}} & 0 \\ 0 & -\dfrac{\hat{R}_r + p\,\hat{\sigma}\,\hat{L}_r + K_{idr}}{K_{idr}} \dfrac{2L_s}{3\omega_e L_m\psi_{ds}} \end{bmatrix} \begin{bmatrix} \omega_r \\ Q_s \end{bmatrix}
\tag{3.121}
$$

$$
+ \begin{bmatrix} -\dfrac{\hat{R}_r + p\,\hat{\sigma}\,\hat{L}_r + K_{iqr}}{K_{iqr}} \dfrac{4L_s T_m}{3PL_m\psi_{ds}} \\ 0 \end{bmatrix}
$$

48

Solving (3.121) gives:

$$\omega_r = \frac{\hat{K}_2}{\hat{K}_1}\omega_r^* + \frac{\hat{K}_3}{\hat{K}_1}T_m \tag{3.122}$$

Where $\hat{K}_1 = \dfrac{2pJL_s}{L_m\psi_{ds}}\dfrac{\hat{R}_r + p\,\hat{\sigma}\,\hat{L}_r + K_{iqr}}{K_{iqr}} + \dfrac{\hat{L}_s\,K_{wr}}{\hat{L}_m\,\psi_{ds}}$

$\hat{K}_2 = \dfrac{\hat{L}_s\,K_{wr}}{\hat{L}_m\,\psi_{ds}}$ and $\hat{K}_3 = \dfrac{\hat{R}_r + p\,\hat{\sigma}\,\hat{L}_r + K_{iqr}}{K_{iqr}}\dfrac{L_s}{L_m\psi_{ds}} - \dfrac{\hat{L}_s}{\hat{L}_m\,\psi_{ds}}$

Similarly,

$$Q_s = \frac{\hat{K}_4}{\hat{K}_5}Q_s^* \tag{3.123}$$

Where $\hat{K}_4 = \dfrac{K_{Qs}}{p\psi_{ds}\,\hat{\sigma}\,\hat{L}_r}$ and $\hat{K}_5 = \dfrac{K_{Qs}}{p\psi_{ds}\,\hat{\sigma}\,\hat{L}_r} - \dfrac{\hat{R}_r + p\,\hat{\sigma}\,\hat{L}_r + K_{idr}}{K_{idr}}\dfrac{2L_s}{3\omega_e L_m\psi_{ds}}$

If the measured parameters are assumed to be equal to the actual quantities, solving (3.121) gives:

$$\omega_r = \frac{K_2}{K_1}\omega_r^* + \frac{K_3}{K_1}T_m \tag{3.124}$$

Where $K_1 = \dfrac{2pJL_s}{L_m\psi_{ds}}\dfrac{R_r + p\sigma L_r + K_{iqr}}{K_{iqr}} + \dfrac{L_s K_{wr}}{L_m\psi_{ds}}$, $K_2 = \dfrac{L_s K_{wr}}{L_m\psi_{ds}}$ and

$K_3 = \dfrac{R_r + p\sigma L_r + K_{iqr}}{K_{iqr}}\dfrac{L_s}{L_m\psi_{ds}} - \dfrac{L_s}{L_m\psi_{ds}}$

Similarly,

$$Q_s = \frac{K_4}{K_5}Q_s^* \tag{3.125}$$

Where $K_4 = \dfrac{K_{Qs}}{p\psi_{ds}\sigma L_r}$ and $K_5 = \dfrac{K_{Qs}}{p\psi_{ds}\sigma L_r} - \dfrac{R_r + p\sigma L_r + K_{idr}}{K_{idr}}\dfrac{2L_s}{3\omega_e L_m\psi_{ds}}$

Here it should be noted that the inner current controller parameters are same for q and d-axis currents, i.e. $K_{iqr} = K_{idr}$.

Similarly, in the GSC, from (3.73):

$$\sigma_{dc} = K_{dc}\left(V_{dc}^* - V_{dc}\right) = \frac{3}{4}\left(M_{qr}I_{qr} + M_{dr}I_{dr}\right) + \frac{3}{4}\left(M_{qf}I_{qf} + M_{df}I_{df}\right) \tag{3.126}$$

$$I_{qf}^* = \frac{1}{M_{qf}}\left(\frac{4}{3}\left(\sigma_{dc} - \frac{3}{4}\left(M_{qr}I_{qr} + M_{dr}I_{dr}\right)\right) - M_{df}I_{df}\right) \quad (3.127)$$

Where $M_{qr} = \dfrac{2V_{qr}^*}{V_{dc}}$ and $M_{dr} = \dfrac{2V_{dr}^*}{V_{dc}}$. Here, $\dfrac{3}{4}\left(M_{qr}I_{qr} + M_{dr}I_{dr}\right)$ is the DC-link current

coming out from RSC.

And we also know from (3.55) and (3.56) that-

$$V_{qr}^* = K_{Iqr}\left(I_{qr}^* - I_{qr}\right) + \omega_{sl}\left(\frac{L_m}{L_s}\psi_{ds} + \sigma L_r I_{dr}\right) \quad (3.128)$$

$$V_{dr}^* = K_{Idr}\left(I_{dr}^* - I_{dr}\right) - \omega_{sl}\sigma L_r I_{qr} \quad (3.129)$$

Using (3.128), (3.129), (3.109) and (3.116), DC-link current is expressed as:

$$\frac{3}{4}\left(M_{qr}I_{qr} + M_{dr}I_{dr}\right) =$$

$$\frac{3}{2V_{dc}}\left[\begin{array}{c} K_{Iqr}K_{wr}\dfrac{p8JL_s}{3P^2L_m\psi_{ds}}\left(\omega_r^*\omega_r - \omega_r^2\right) - \dfrac{4T_mL_s}{3PL_m\psi_{ds}}K_{Iqr}K_{wr}\left(\omega_r^* - \omega_r\right) + \dfrac{\omega_{sl}p8J\omega_r}{3P^2} \\[3mm] -\dfrac{\omega_{sl}4T_m}{3P} + \dfrac{2L_sK_{Idr}K_{Qs}}{3p\sigma L_r\omega_e L_m\psi_{ds}^2}\left(Q_sQ_s^* - Q_s^2\right) - \dfrac{4L_s^2K_{Idr}}{9\omega_e^2L_m^2\psi_{ds}^2} \end{array}\right] \quad (3.130)$$

Here, ψ_{ds} is regulated to constant value using flux control. Hence, it is clear from (3.130) that the DC-current flowing in ac/dc/ac converter has a non-linear relationship between control variables like ω_r, Q_s and V_{dc}. So it can be concluded that decoupled control of Q_f, Q_s, ω_r and V_{dc} can be done if the DC-link current coming out from RSC is taken as a disturbance for the GSC control.

Now, from (3.86):

$$\begin{cases} \sigma_{Qf} = \left(V_{df} - \hat{R}_f I_{df} + \hat{\omega}_e \hat{L}_f I_{qf}\right) \\[3mm] \sigma_{Qf} = \left(\hat{R}_f I_{df} + p\hat{L}_f I_{df} - \hat{\omega}_e \hat{L}_f I_{qf} - \hat{R}_f I_{df} + \hat{\omega}_e \hat{L}_f I_{qf}\right) \\[3mm] I_{df}^* = \dfrac{\sigma_{Qf}}{p\hat{L}_f} \end{cases} \quad (3.131)$$

From (3.131) and (3.127):

$$I_{qf}^* = \frac{1}{M_{qf}}\left(\frac{4}{3}\left(\sigma_{dc} - \frac{3}{4}\left(M_{qr}I_{qr} + M_{dr}I_{dr}\right)\right) - M_{df}\frac{\sigma_{Qf}}{p\hat{L}_f}\right) \quad (3.132)$$

Combining (3.132) and (3.127) gives:

$$\begin{bmatrix} I_{qf}^* \\ I_{df}^* \end{bmatrix} = \underbrace{\begin{bmatrix} \dfrac{4}{3M_{qf}} & -\dfrac{M_{df}}{p\hat{L}_f M_{qf}} \\ 0 & \dfrac{1}{p\hat{L}_f} \end{bmatrix}}_{O} \begin{bmatrix} \sigma_{dc} \\ \sigma_{Qf} \end{bmatrix} + \underbrace{\begin{bmatrix} -\dfrac{1}{M_{qf}}\left(M_{qr}I_{qr} + M_{dr}I_{dr}\right) \\ 0 \end{bmatrix}}_{P} \tag{3.133}$$

From (3.72):

$$CpV_{dc} = \frac{3}{4}\left(M_{qr}I_{qr} + M_{dr}I_{dr}\right) + \frac{3}{4}\left(M_{df}I_{df} + M_{qf}I_{qf}\right) \tag{3.134}$$

$$I_{qf} = \frac{4}{3M_{qf}}\left(CpV_{dc} - \frac{3}{4}\left(M_{qr}I_{qr} + M_{dr}I_{dr}\right)\right) - \left(\frac{M_{df}}{M_{qf}}I_{df}\right) \tag{3.135}$$

From (3.84):

$$pQ_f = \frac{3V_{qs}}{2L_f}\left(V_{df} - R_f I_{df} + \omega_e L_f I_{qf}\right) \tag{3.136}$$

$$\begin{cases} pQ_f = \dfrac{3V_{qs}}{2L_f}\left(R_f I_{df} + pL_f I_{df} - \omega_e L_f I_{qf} - R_f I_{df} + \omega_e L_f I_{qf}\right) \\[2mm] I_{df} = \dfrac{2Q_f}{3V_{qs}} \end{cases} \tag{3.137}$$

Substituting (3.137) into (3.135):

$$I_{qf} = \frac{4}{3M_{qf}}\left(CpV_{dc} - \frac{3}{4}\left(M_{qr}I_{qr} + M_{dr}I_{dr}\right)\right) - \left(\frac{2M_{df}}{3M_{qf}}\frac{Q_f}{V_{qs}}\right) \tag{3.138}$$

Combining (3.138) and (3.137)

$$\begin{bmatrix} I_{qf} \\ I_{df} \end{bmatrix} = \underbrace{\begin{bmatrix} \dfrac{4}{3M_{qf}}pC & -\dfrac{2M_{df}}{3M_{qf}V_{qs}} \\ 0 & \dfrac{2}{3V_{qs}} \end{bmatrix}}_{Q} \begin{bmatrix} V_{dc} \\ Q_f \end{bmatrix} + \underbrace{\begin{bmatrix} -\dfrac{1}{M_{qf}}\left(M_{qr}I_{qr} + M_{dr}I_{dr}\right) \\ 0 \end{bmatrix}}_{R} \tag{3.139}$$

From (3.92):

$$\left(\hat{R}_f + p\hat{L}_f\right)I_{qf} = K_{iqf}I_{qf}^* - K_{iqf}I_{qf} \tag{3.140}$$

From (3.93):

$$\left(\hat{R}_f + p\hat{L}_f\right)I_{df} = K_{idf}I_{df}^* - K_{idf}I_{df} \tag{3.141}$$

Combining (3.140) and (3.141) gives:

51

$$
\begin{bmatrix} I_{qf}^* \\ I_{df}^* \end{bmatrix} = \underbrace{\begin{bmatrix} \dfrac{\hat{R}_f + p\hat{L}_f + K_{iqf}}{K_{iqf}} & 0 \\ 0 & \dfrac{\hat{R}_f + p\hat{L}_f + K_{idf}}{K_{idf}} \end{bmatrix}}_{F} \begin{bmatrix} I_{qf} \\ I_{df} \end{bmatrix}
\tag{3.142}
$$

Substituting (3.132) and (3.139) in (3.142):

$$
O\begin{bmatrix} \sigma_{dc} \\ \sigma_{Qf} \end{bmatrix} + P = FQ\begin{bmatrix} V_{dc} \\ Q_f \end{bmatrix} + FR
\tag{3.143}
$$

$$
\begin{bmatrix} \dfrac{4}{3M_{qf}} & -\dfrac{M_{df}}{p\hat{L}_f M_{qf}} \\ 0 & \dfrac{1}{p\hat{L}_f} \end{bmatrix} \begin{bmatrix} K_{dc}\left(V_{dc}^* - V_{dc}\right) \\ K_{Qf}\left(Q_f^* - Q_f\right) \end{bmatrix} + \begin{bmatrix} -\dfrac{1}{M_{qf}}\left(M_{qr}I_{qr} + M_{dr}I_{dr}\right) \\ 0 \end{bmatrix}
$$

$$
= \begin{bmatrix} \dfrac{4pC}{3M_{qf}}\dfrac{\hat{R}_f + p\hat{L}_f + K_{iqf}}{K_{iqf}} & -\dfrac{2M_{df}}{3V_{qs}M_{qf}}\dfrac{\hat{R}_f + p\hat{L}_f + K_{iqf}}{K_{iqf}} \\ 0 & \dfrac{2}{3V_{qs}}\dfrac{\hat{R}_f + p\hat{L}_f + K_{idf}}{K_{idf}} \end{bmatrix} \begin{bmatrix} V_{dc} \\ Q_f \end{bmatrix} + \begin{bmatrix} -\dfrac{\left(M_{qr}I_{qr} + M_{dr}I_{dr}\right)\hat{R}_f + p\hat{L}_f + K_{iqf}}{M_{qf}}\dfrac{}{K_{iqf}} \\ 0 \end{bmatrix}
\tag{3.144}
$$

Solving (3.144) gives:

$$
V_{dc} = \frac{K_{dc}}{\hat{\tau}_1}V_{dc}^* - \frac{3}{4}\frac{\hat{\gamma}_f - 1}{\hat{\tau}_1}\left(M_{qr}I_{qr} + M_{dr}I_{dr}\right)
\tag{3.145}
$$

Where $\hat{\gamma}_f = \dfrac{\hat{R}_f + p\hat{L}_f + K_{idf}}{K_{idf}}$ and $\hat{\tau}_1 = pC\hat{\gamma}_f + K_{dc}$.

Similarly, $Q_f = \dfrac{\hat{\eta}_1}{\hat{\eta}_2}Q_f^*$
$\tag{3.146}$

Where $\hat{\eta}_1 = \dfrac{K_{Qf}}{p\hat{L}_f}$ and $\hat{\eta}_2 = \hat{\gamma}_f\dfrac{2}{3V_{qs}} + \dfrac{K_{Qf}}{p\hat{L}_f}$

If the measured quantities are assumed to be equal to the actual quantities, solving (3.144) gives:

$$
V_{dc} = \frac{K_{dc}}{\tau_1}V_{dc}^* - \frac{3}{4}\frac{\gamma_f - 1}{\tau_1}\left(M_{qr}I_{qr} + M_{dr}I_{dr}\right)
\tag{3.147}
$$

Where $\gamma_f = \dfrac{R_f + pL_f + K_{idf}}{K_{idf}}$ and $\tau_1 = pC\gamma_f + K_{dc}$

Similarly, $Q_f = \dfrac{\eta_1}{\eta_2}Q_f^*$ (3.148)

Where $\eta_1 = \dfrac{K_{Qf}}{sL_f}$ and $\eta_2 = \gamma_f \dfrac{2}{3V_{qs}} + \dfrac{K_{Qf}}{pL_f}$

Here it should be noted that the inner current controller parameters are same for q and d-axis currents, i.e. $K_{iqf} = K_{idf}$.

Combining (3.122), (3.123), (3.145) and (3.146) gives:

$$
\begin{bmatrix} \omega_r \\ Q_s \\ V_{dc} \\ Q_f \end{bmatrix} = \underbrace{\begin{bmatrix} \hat{K}_{11} & 0 & 0 & 0 \\ 0 & \hat{K}_{22} & 0 & 0 \\ 0 & 0 & \hat{K}_{33} & 0 \\ 0 & 0 & 0 & \hat{K}_{44} \end{bmatrix}}_{A} \begin{bmatrix} \omega_r^* \\ Q_s^* \\ V_{dc}^* \\ Q_f^* \end{bmatrix} + \begin{bmatrix} \hat{\sigma}_{11} \\ 0 \\ 0 \\ 0 \end{bmatrix} + \begin{bmatrix} 0 \\ 0 \\ \hat{\mu}_{33} \\ 0 \end{bmatrix}
$$
    (3.149)

Where $\hat{K}_{11} = \dfrac{\hat{K}_2}{\hat{K}_1}, \hat{K}_{22} = \dfrac{\hat{K}_4}{\hat{K}_5}, \hat{K}_{33} = \dfrac{\hat{K}_{dc}}{\hat{\tau}_1}, \hat{K}_{44} = \dfrac{\hat{\eta}_1}{\hat{\eta}_2}, \hat{\sigma}_{11} = \dfrac{\hat{K}_3}{\hat{K}_1}$ and

$$
\hat{\mu}_{33} = \frac{3}{2V_{dc}}\frac{\hat{\gamma}_f - 1}{\hat{\tau}_1}\left[\begin{array}{c} K_{Iqr}K_{wr}\dfrac{p8JL_s}{3P^2 L_m \psi_{ds}}\left(\omega_r^*\omega_r - \omega_r^2\right) - \dfrac{4T_m L_s}{3PL_m \psi_{ds}}K_{Iqr}K_{wr}\left(\omega_r^* - \omega_r\right) + \dfrac{\omega_{sl}p8J\omega_r}{3P^2} \\[3mm] -\dfrac{\omega_{sl}4T_m}{3P} + \dfrac{2L_s K_{Idr}K_{Qs}}{3p\sigma L_r \omega_e L_m \psi_{ds}^2}\left(Q_s^* Q_s - Q_s^2\right) - \dfrac{4L_s^2 K_{Idr}}{9\omega_e^2 L_m^2 \psi_{ds}^2} \end{array} \right]
$$

Combining (3.124), (3.125), (3.147) and (3.148) gives:

$$
\begin{bmatrix} \omega_r \\ Q_s \\ V_{dc} \\ Q_f \end{bmatrix} = \underbrace{\begin{bmatrix} K_{11} & 0 & 0 & 0 \\ 0 & K_{22} & 0 & 0 \\ 0 & 0 & K_{33} & 0 \\ 0 & 0 & 0 & K_{44} \end{bmatrix}}_{\theta} \begin{bmatrix} \omega_r^* \\ Q_s^* \\ V_{dc}^* \\ Q_f^* \end{bmatrix} + \begin{bmatrix} \sigma_{11}T_m \\ 0 \\ 0 \\ 0 \end{bmatrix} + \begin{bmatrix} 0 \\ 0 \\ \mu_{33} \\ 0 \end{bmatrix}
$$
    (3.150)

Where $K_{11} = \dfrac{K_2}{K_1}, K_{22} = \dfrac{K_4}{K_5}, K_{33} = \dfrac{K_{dc}}{\tau_1}, K_{44} = \dfrac{\eta_1}{\eta_2}, \sigma_{11} = \dfrac{K_3}{K_1}$ and

$$
\mu_{33} = \frac{3}{2V_{dc}}\frac{\gamma_f - 1}{\hat{\tau}_1}\left[\begin{array}{c} K_{Iqr}K_{wr}\dfrac{p8JL_s}{3P^2 L_m \psi_{ds}}\left(\omega_r^*\omega_r - \omega_r^2\right) - \dfrac{4T_m L_s}{3PL_m \psi_{ds}}K_{Iqr}K_{wr}\left(\omega_r^* - \omega_r\right) + \dfrac{\omega_{sl}p8J\omega_r}{3P^2} \\[3mm] -\dfrac{\omega_{sl}4T_m}{3P} + \dfrac{2L_s K_{Idr}K_{Qs}}{3p\sigma L_r \omega_e L_m \psi_{ds}^2}\left(Q_s^* Q_s - Q_s^2\right) - \dfrac{4L_s^2 K_{Idr}}{9\omega_e^2 L_m^2 \psi_{ds}^2} \end{array} \right]
$$

As shown in (3.149) and (3.150), the transfer function matrices A and are both diagonal which verifies that all the four controlled quantities are independent of each other regardless of error in parameter estimation. That means, the controller design can be done independent of each other and combined them together for the overall control. According to (3.149) and (3.150), there exists a non-linear relation through the DC-link voltage controller which can be considered as a disturbance for the GSC control.

3.4 Phase Locked Loop (PLL)

A PLL is designed to define the reference angle for qd transformation so that the stator voltage can be aligned along the q-axis and is included in the overall model of the system to make the designed system more realistic. Figure 3.4 shows the 3-phase PLL which takes the input as the measured DFIG terminal voltage V_s and transforms it to qd-reference frame. PLL aligns the stator side voltage to q-axis by comparing d-axis load voltage with zero reference voltage. The voltage error signal is delivered through the PI controller to obtain the angular frequency of the terminal bus voltage.
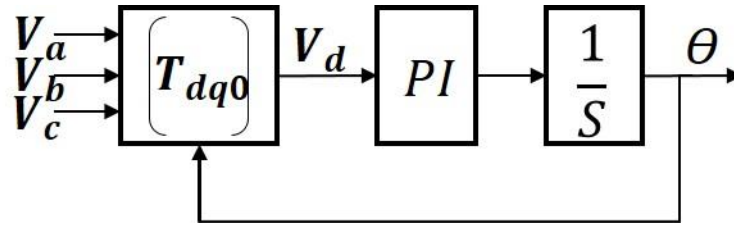
Figure 3.4 Block diagram of PLL control

Hence in the PLL system:

$$V_{ds} = -V_s \sin\left(\theta_i - \theta_s\right) \Rightarrow 0 = -V_s \sin\left(\theta_i - \theta_s\right) \Rightarrow \theta_i = \theta_s \tag{3.151}$$

Now the error signal is given as: $e = 0 - V_{ds} = V_s \sin\left(\theta_i - \theta_s\right)$

If $\left(\theta_i - \theta_s\right)$ is very small, then we can write: $\sin\left(\theta_i - \theta_s\right) \approx \left(\theta_i - \theta_s\right)$

From the block diagram in Figure 3.4, $V_s\left(\theta_i - \theta_s\right)$ is the input to the controller and ω_e is the output from the controller. Hence,

$$\begin{cases} V_s\left(\theta_i - \theta_s\right)K_{pll} = \omega_e \\ \dfrac{1}{V_s} p\theta_s = \left(\theta_i - \theta_s\right)K_{pll} = \sigma_\theta \end{cases} \tag{3.152}$$

Where $K_{pll} = K_{P\_pll} + \dfrac{K_{I\_pll}}{p}$

$$\frac{1}{V_s} p\theta_s = \left(K_{P\_pll} + \frac{K_{I\_pll}}{p} \right)\theta_i - \left(K_{P\_pll} + \frac{K_{I\_pll}}{p} \right)\theta_s \qquad (3.153)$$

$$\frac{\theta_s}{\theta_i} = \frac{pV_s K_{P\_pll} + V_s K_{I\_pll}}{p^2 + pV_s K_{P\_pll} + V_s K_{I\_pll}} \qquad (3.154)$$

Now matching the denominator of (3.154) with the Butterworth second order polynomial $p^2 + \sqrt{2}\omega_{0\_pll}\,p + \omega_{0\_pll}^2$, the parameters of the controller are:

$$K_{P\_pll} = \frac{\sqrt{2}\omega_{0\_pll}}{V_s} \qquad (3.155)$$

$$K_{I\_pll} = \frac{\omega_{0\_pll}^2}{V_s} \qquad (3.156)$$

Where ω_{0_pll} is the bandwidth frequency of the PLL controller.

The PI controllers values used for the simulation study following above procedure. The switching frequency is taken as 1 kHz and the bandwidth of inner current controller is taken ten times that of outer loop controller, i.e.

$$\omega_{sw} = 2 * \pi * f_{sw} = 6280 \text{ rad/sec and } \omega_{inner} = \frac{\omega_{sw}}{10}\,;\ \omega_{outer} = \frac{\omega_{inner}}{10}$$

$\omega_{inner} = \omega_0 = \omega_{oc} = 628$ rad/sec, $\omega_{outer} = \omega_{odc} = \omega_{oQs} = \omega_{oQf} = 62.8$ rad/sec and $\omega_{owr} = 0.628$ rad/s

From (3.66): $K_{qp} = K_{dp} = \sqrt{2}\omega_0\sigma L_r - R_r = 1.76$ and from (3.67): $K_{qi} = K_{di} = \sigma L_r \omega_0^2 = 783.6$

From (3.68): $K_{Pwr} = \sqrt{2}\omega_{0wr}\dfrac{2J}{P} = 8.26$ and from (3.69): $K_{Iwr} = \dfrac{2J}{P}\omega_{0wr}^2 = 3.65$

From (3.77): $K_{Pdc} = \sqrt{2}\omega_{0dc}C_{dc} = 5.32$ and from (3.78): $K_{Idc} = \omega_{0dc}^2 C_{dc} = 236.63$

From (3.97): $K_{P1} = \sqrt{2}\omega_{0C}L_f - R_f = 1.77$ and from (3.98): $K_{I1} = \omega_{0C}^2 L_f = 788.76$

From (3.70): $K_{PQs} = \sqrt{2}\omega_{0Qs}\Delta = 0.00022$ and from (3.71): $K_{IQs} = \omega_{Qs}^2 \Delta = 0.001$

From (3.89): $K_{PQf} = \sqrt{2}\omega_{0Qf}\Gamma = 0.0002$ and from (3.90): $K_{IQf} = \omega_{0Qf}^2 \Gamma = 0.0093$

In PLL controller design, the switching frequency is taken as 2 kHz and the bandwidth of the PLL controller is taken as: $\omega_{sw} = 2 * \pi * f_{sw} = 12560$ rad/sec and $\omega_0 = \dfrac{\omega_{sw}}{15} = 837.3$ rad/sec

From (3.155): $K_{P\_pll} = \dfrac{\sqrt{2}\omega_{0\_pll}}{V_s} = 2.10$ and from (3.156): $K_{I\_pll} = \dfrac{\omega_{0\_pll}^2}{V_s} = 1244.4$

3.5   Simulation Results

Here, the profiles of the rotor and stator currents in the ABC frame are shown in Figure 3.5 and Figure 3.6, respectively. As shown in Figure 3.5 and Figure 3.6, the frequency of the stator currents is much higher than the rotor currents due to the reason that $f_r = sf_s$ where, s, is the slip.
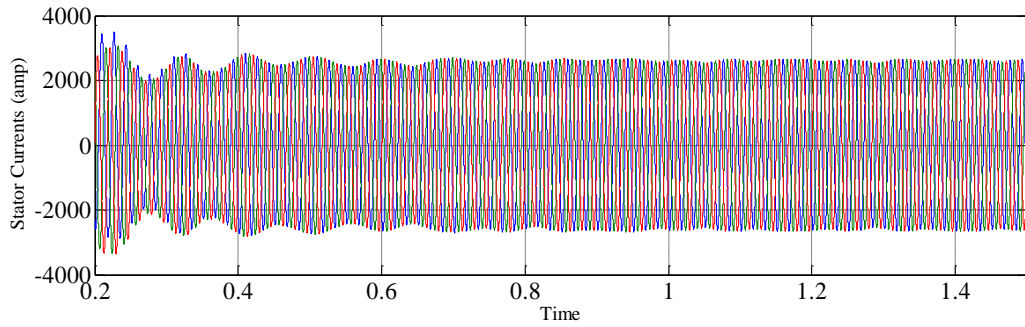

**Figure 3.5 Stator phase current profiles. (ABC reference frame)**
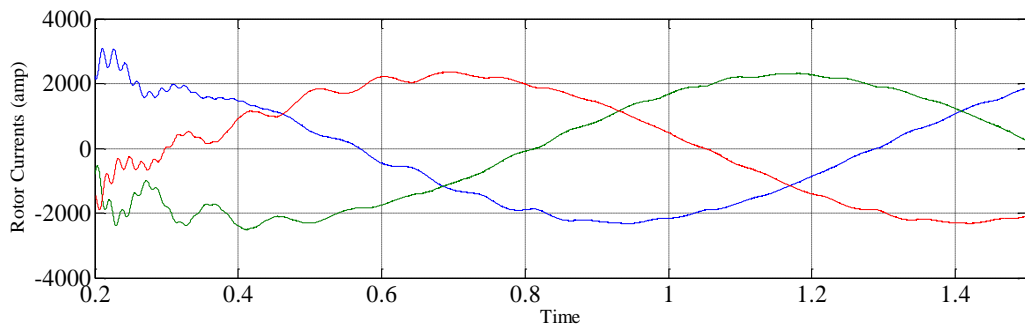
Figure 3.6 Rotor phase current profiles. (ABC reference frame)

The electromagnetic torque in Figure 3.7 is also controlled by the rotor quadrature axis current. One can easily reach this conclusion through using equation (3.38). In Figure 3.8, the grid-side converter controller will attempt to maintain the DC-link voltage at 1200 volt. In this simulation, the ripple voltage across the capacitor was found to be as follows from Figure 3.9:
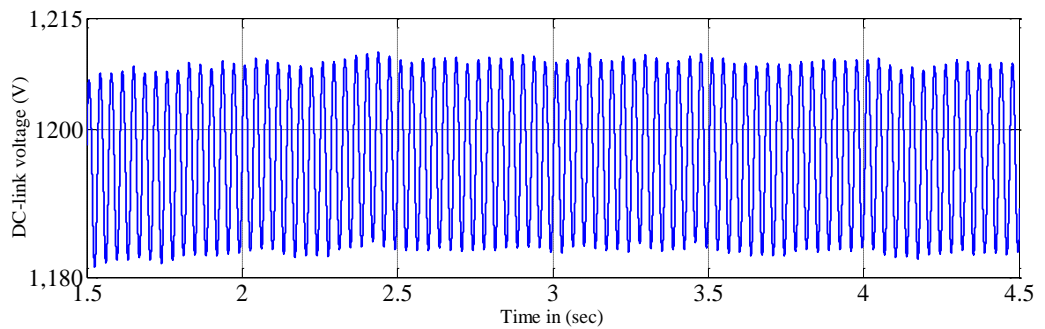
$$\text{Ripple} = \frac{1210 - 1180}{1200} = 2.5\%$$
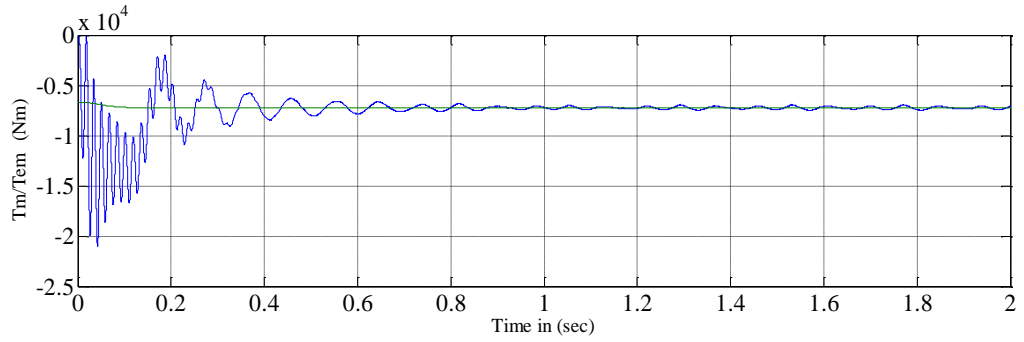
**Figure 3.7 Mechanical torque vs Electromagnetic torque profiles**
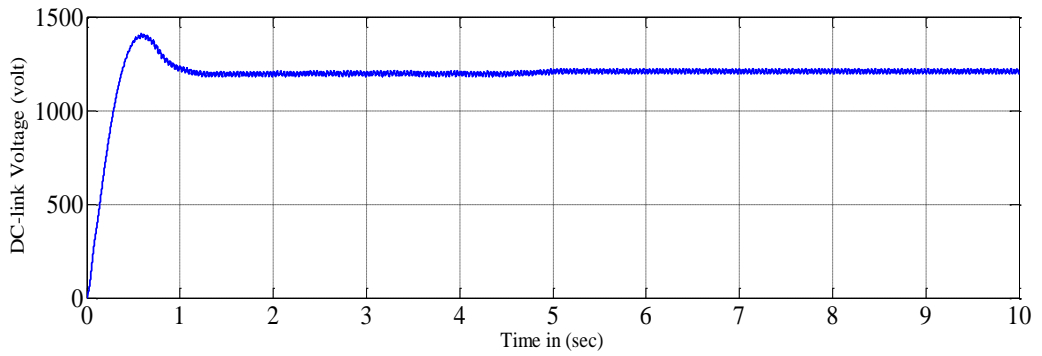
**Figure 3.8 DC-link voltage profile**

Figure 3.9 DC-link ripple voltage profile

Figure 3.10 shows the plot of stator voltages in q and d axis. The stator voltage is aligned along q-axis using the reference angle given by PLL and the d-axis stator voltage is regulated to be zero. Figure 3.11 shows the plot of stator fluxes in q and d axis. The q-axis stator flux is regulated to be zero and d-axis flux gives the total stator flux.
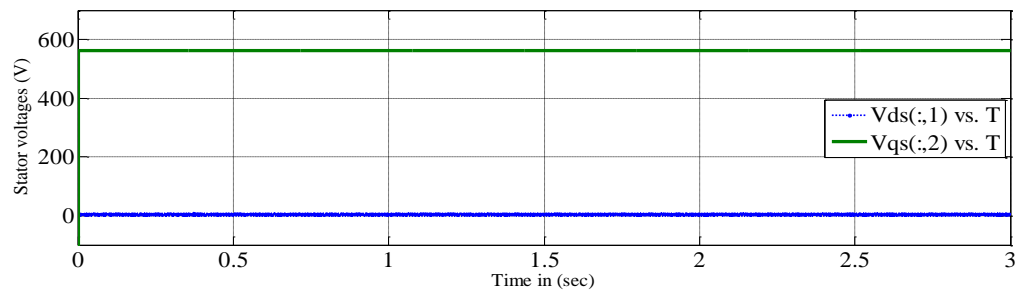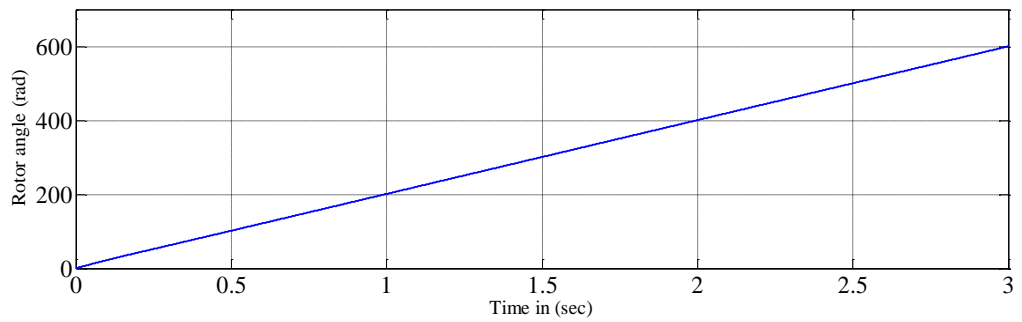

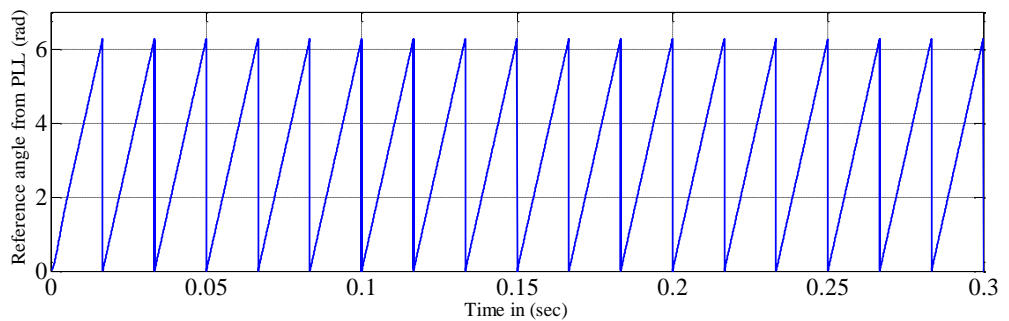**Figure 3.10 Stator voltage profiles (DQ reference frame)**
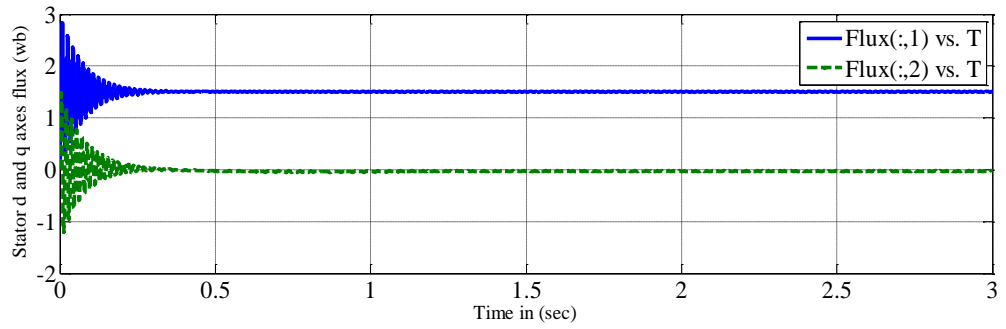
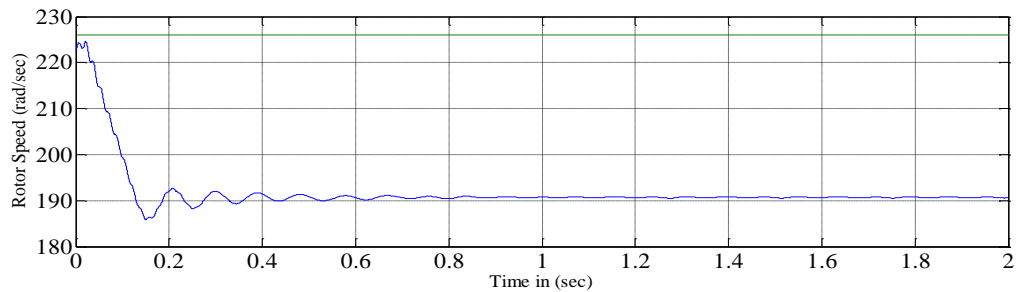**Figure 3.11 Stator flux profiles (DQ reference frame)**

Figure 3.12 and 3.13 show the plot of reference angle given by PLL to align the stator voltage along the q-axis. Figure 3.14 and 3.15 show the plot of rotor speed and synchronous speed respectively.
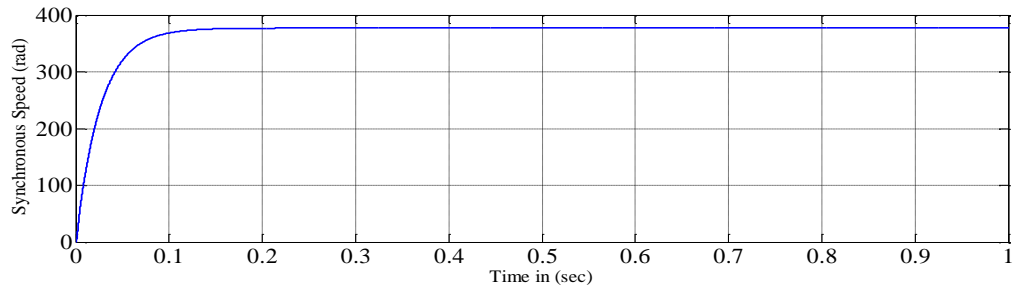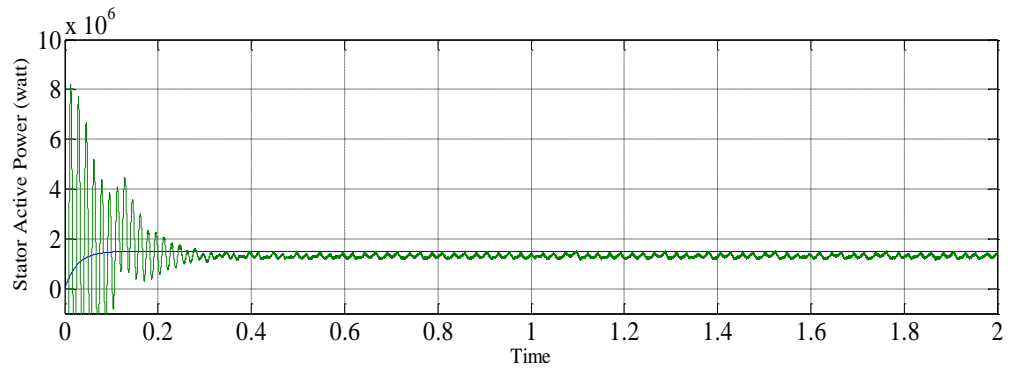

Figure 3.12 Rotor angle

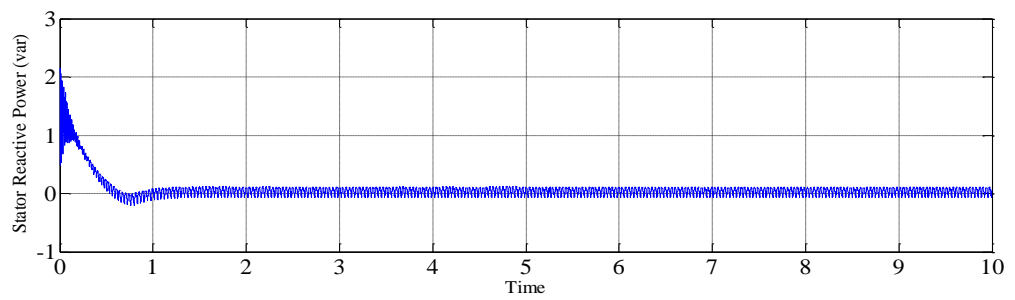**Figure 3.13 Reference angle output from PLL**

Figure 3.14 Rotor speed

58

Figure 3.15 Synchronous speed

Figure 3.16 Stator active power
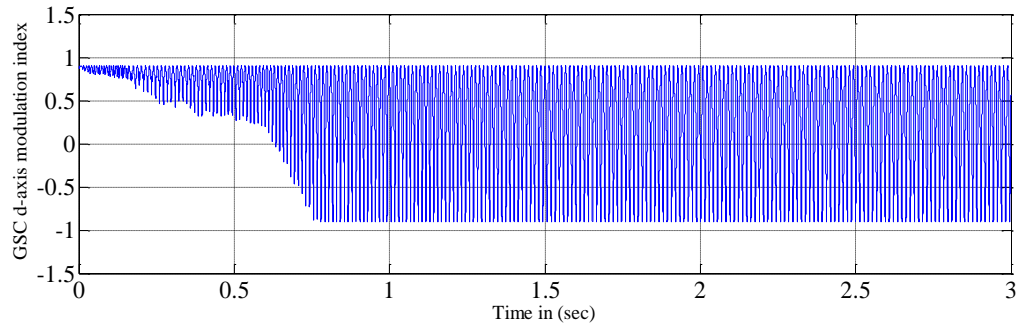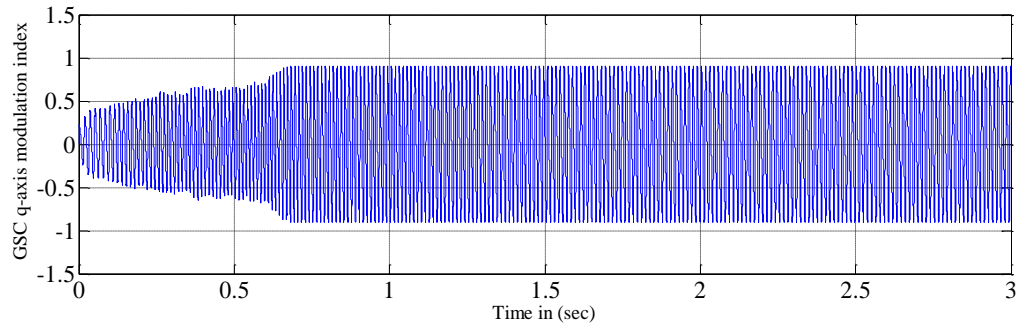

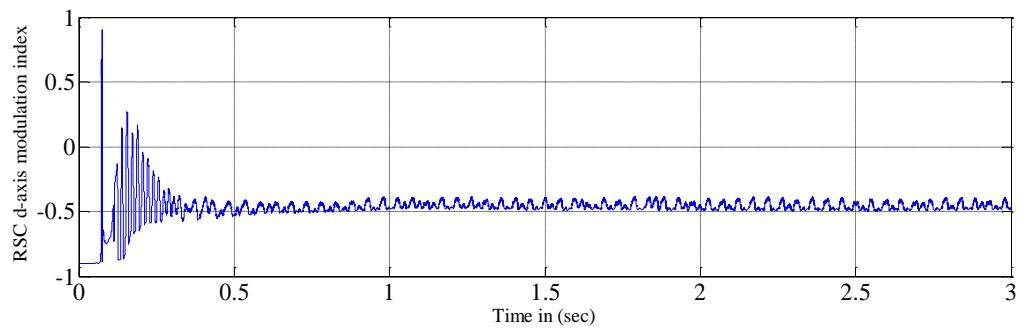**Figure 3.17 Stator reactive power**
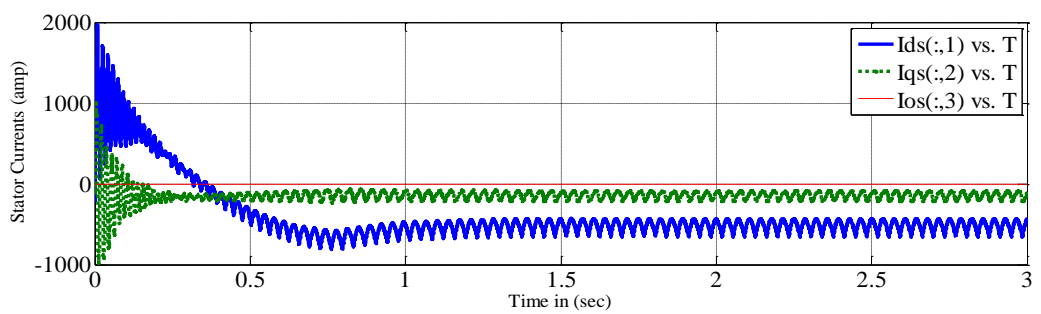
Figure 3.18 Stator current profiles (DQ reference frame)
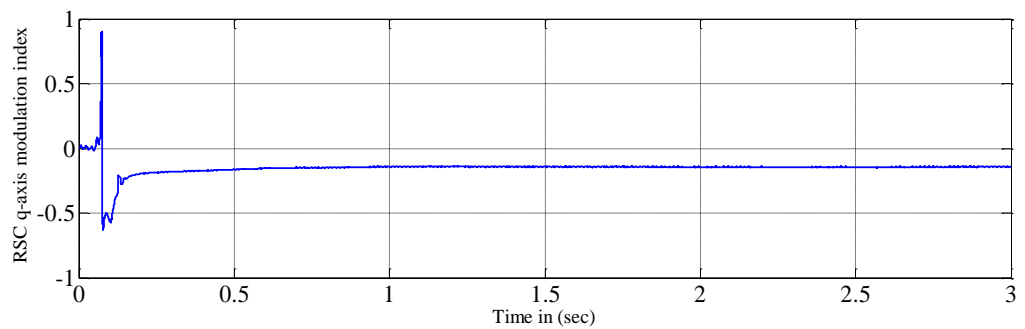
Figure 3.19 GSC d-axis modulation index

Figure 3.20 GSC q-axis modulation index

Figure 3.21 RSC d-axis modulation index

Figure 3.22 RSC q-axis modulation index

Figure 3.19 to 3.22 show the plot of GSC and RSC, dq-axes modulation indexes respectively.

Chapter 4

Conclusions and Future Scope

A detailed simulation model of a DFIG-based wind turbine system is developed for the 1.5 MW wind turbine connected to the power grid. All of the primary components are modelled including the aerodynamic system of wind turbine, DFIG, rotor mechanical system, the overall control system, and the power grid. The stator side flux estimator is designed using a PLL system is embedded with the DFIG model which gives the reference angle to align the stator side voltage along the q-axis.

In this thesis, the modelling and control of a doubly-fed induction generator based wind turbine-generator system have been considered. More specifically, the modelling of different components, the control strategies for the back-to-back converter have been studied and analysed in detail.

As a basis of the research, the model of a wind turbine-generator system equipped with a doubly-fed induction generator was developed in a Matlab/Simulink environment, which simulates the dynamics of the system from the turbine rotor, where the kinetic wind energy is converted to the mechanical energy, to the generator, which transforms the mechanical power to electrical power, and then to the grid connection point, where the electric power is fed into the grid. The model of the wind turbine system includes the aerodynamic models of the wind turbine, the drive train system models, the back-to-back converter models, and the doubly-fed induction generator models.

Four control schemes were implemented in the wind turbine system, which are, the generator-side converter control, the grid-side converter control, the pitch angle control and the maximum power point tracking control, respectively. The objective of the vector-control scheme for the grid-side converter controller is used to maintain the constant voltage across the capacitor and produce a unity power factor operation of the grid. The vector control scheme for the generator-side

converter controller is used to regulating the torque, active power and reactive power.

Some subjects for future studies are listed as follows:

- Wind speed sensor-less control strategies should be studied, due to the fact that the anemometer may not accurately measure the wind speed.
- Direct torque control and direct power control should be considered, because of the advantages of no current regulators, no coordinate transformations and specific modulations, and no current control loops.
- Matrix converters are another interesting topic because of their ac to ac transformation ability.
- The transient behaviours of the DFIG-based wind turbine system under disturbances of grid failures should be studied.

REFERENCES

1. Wei Qiao, "Integrated Control of Wind Farms, FACTS Devices and the Power Network Using Neural Networks and Adaptive Critic Designs", Georgia Institute of Technology, Ph.D. dissertation, July 2008.

2. Singh, Bhim, Shiv Kumar Aggarwal, and Tara Chandra Kandpal. "Performance of Wind Energy Conversion System Using a Doubly Fed Induction Generator for Maximum Power Point Tracking", *IEEE Industry Applications Society Annual Meeting,* vol. 139, no. 5, pp. 429-442, July 2010.

3. Jin Yang, "Fault Analysis and Protection for Wind Power Generation Systems", University of Glasgow, Ph.D. dissertation, March 2011.

4. Raymond W. Flumerfelt and Su Su Wang, "Wind turbines," in AccessScience, ©McGraw-Hill Companies, 2009, http://www.accessscience.com.

5. Bijaya Pokharel, "Modeling, Control and Analysis of a Doubly Fed Induction Generator Based Wind Turbine System with Voltage Regulation", Tennessee Technological University, Master thesis, December 2011.

6. F. Iov, M. Ciobotaru and F. Blaabjerg, "Power Electronics Control of Wind Energy in Distributed Power Systems", *11th International Conference on Optimization of Electrical and Electronic Equipment*, Brasov, pp. XXIX - XLIV, May 2008.

7. S. Muller, M. Deicke and Rik W. De Doncker, "Doubly fed induction generator systems for wind turbines", *IEEE Industry Applications Magazine*, Vol. 8, No. 3, pp. 26-33, May/June 2002.

8. S. Benelghali, M. E. H. Benbouzid and J. F. Charpentier, "Comparison of PMSG and DFIG for Marine Current Turbine Applications", *XIX International Conference on Electrical Machines*, pp. 1-6, Rome, September 2010.

9. H. Li and Z. Chen, "Overview of Different Wind Generator Systems and Their Comparisons", *IET Renewable Power Generation*, Vol. 2, No. 2, pp.123-138, August 2008.

10. "Wind Speed and Wind Energy", Available on line: http://energybible.com/wind_energy/wind_speed.html.

11. Abram Perdana, "Dynamic Models of Wind Turbines", Ph.D. dissertation, Chalmers University of Technology, Sweden, 2008.

12. Tao Sun, "Power Quality of Grid-Connected Wind Turbines with DFIG and Their Interaction with the Grid", Ph.D. dissertation, Aalborg University, Denmark, May 2004.

13. Iulian Munteanu, Antoneta Iuliana Bratcu, Nicolaos-Antonio Cutululis and Emil Ceanga, "Optimal Control of Wind Energy System", London, Springer, 2008.

14. Ming Yin, Gengyin Li, Ming Zhou and Chengyong Zhao, "Modeling of the Wind Turbine with a Permanent Magnet Synchronous Generator for Integration", *IEEE Power Engineering Society General Meeting*, pp.1-6, Tampa, June 2007.

15. J. G. Slootweg, S. W. H. de Haan, H. Polinder and W. L. Kling, "General Model for Representing Variable Speed Wind Turbines in Power System Dynamics Simulations", *IEEE Transactions on Power Systems*, Vol.18, No.1, pp.144-151, February 2003.

16. N. Miller, W. Price, and J. Sanchez-Gasca, "Dynamic modeling of GE 1.5 and 3.6 wind turbine-generators", General Electric Company, Technical Report, October 2003.

17. Md. Arifujjaman, "Modeling, Simulation and Control of Grid Connected Permanent Magnet Generator (PMG)-based Small Wind Energy Conversion System", *2010 IEEE Electric Power and Energy Conference (EPEC)*, pp.1-6, Halifax, August 2010.

18. S. M. Muyeen, Md. Hasan Ali, R. Takahashi, T. Murata, J. Tamura, Y. Tomaki, A. Sakahara and E. Sasano, "Comparative Study on Transient Stability Analysis of Wind Turbine Generator System Using Different Drive Train Models", *IET Renewable Power Generation*, Vol. 1, No, 2, pp. 131-141, June 2007.

19. Stavros A. Papathanassiou and Michael P. Papadopoulos, "Mechanical Stresses in Fixed-Speed Wind Turbines Due to Network Disturbances", *IEEE Transactions on Energy Conversion*, Vol. 16, No. 4, pp. 361-367, December 2001.

20. R. Melıcio, V. M. F. Mendes and J. P. S. Catalaõ, "Harmonic Assessment of Variable-Speed Wind Turbines Considering a Converter Control Malfunction", *IET Renewable Power Generation*, Vol. 4, No. 2, pp. 139-152, March 2010.

21. H. Li and Z. Chen, "Transient Stability Analysis of Wind Turbines with Induction Generators Considering Blades and Shaft Flexibility", *33rd Annual Conference of the IEEE Industrial Electronics Society*, Chongqing, China, pp. 1604 - 1609, November 2007.

22. Gnanasambandapillai Ramtharanand and Nicholas Jenkins, "Influence of Rotor Structural Dynamics Representations on the Electrical Transient Performance of FSIG and DFIG Wind Turbines", *Wind Energy*, Vol.10, No. 4, pp. 293-301, August 2007.

23. Boubekeur Boukhezzar and Houria Siguerdidjane, "Nonlinear Control of a Variable-Speed Wind Turbine Using a Two-Mass Model", *IEEE Transactions on Energy Conversion*, Vol. 26, No. 1, pp.149-162, March 2011.

24. Wei Qiao, Wei Zhou, José M. Aller, and Ronald G. Harley, "Wind Speed Estimation Based Sensorless Output Maximization Control for a Wind Turbine Driving a DFIG", *IEEE Transactions on Power Electronics*, Vol. 23, No. 3, pp. 1156-1169, May 2008.

25. Lucian Mihet-Popa, Frede Blaabjergand and Ion Boldea, "Wind Turbine Generator Modeling and Simulation Where Rotational Speed is the Controlled Variable", *IEEE Transactions on Industry Applications*, Vol. 30, No.1, pp. 3-10, January/February 2004.

26. Francoise Mei and Bikash Pal, "Modal Analysis of Grid-Connected Doubly Fed Induction Generators", *IEEE Transactions on Energy Conversion*, Vol. 22, No.3, pp. 728-736, September 2007.

27. Tomas Petru and Torbjörn Thiringer, "Modeling of Wind Turbines for Power System Studies", *IEEE Transactions on Power Systems*, Vol. 17, No. 4, pp. 1132-1139, November 2002.

28. G. Quinonez-Varela and A. Cruden, "Modeling and Validation of a Squirrel Cage Induction Generator Wind Turbine during Connection to the Local Grid", *IET Generation, Transmission & Distribution*, Vol.2, No.2, pp. 301-309, March 2008.

29. Chen Wang and George Weiss, "Integral Input-to-State Stability of the Drive-Train of a Wind Turbine", *Proceedings of the 46th IEEE Conference on Decision and Control*, New Orleans, LA, USA, pp.6100-6105, December 2007.

30. Yazhou Lei, Alan Mullane, Gordon Lightbody, and Robert Yacamini, "Modeling of the Wind Turbine With a Doubly Fed Induction Generator for Grid Integration Studies", *IEEE Transactions on Energy Conversion*, Vol. 21, No. 1, pp. 257-264, March 2006.

31. Janaka B. Ekanayake, Lee Holdsworth, Xueguang Wu and Nicholas Jenkins "Dynamic Modeling of Doubly Fed Induction Generator Wind Turbines", *IEEE Transactions on Power Systems*, Vol.18, No.2, pp. 803-809, May 2003.

32. L. J. Ontiveros, P. E. Mercado and G. O. Suvire, "A New Model of the Double-Feed Induction Generator Wind Turbine", *2010 IEEE Transmission and Distribution Conference and Exposition*, Latin America, pp. 263-269, November 2010.

33. Daniel J. Trudnowski, Andrew Gentile, Jawad M. Khan, and Eric M. Petritz, "Fixed-Speed Wind-Generator and Wind-Park Modeling for Transient Stability Studies", *IEEE Transactions on Power Systems*, Vol. 19, No. 4, pp. 1911-1917, November 2004.

34. Andreas Petersson, "Analysis, Modeling and Control of Doubly-Fed Induction Generators for Wind Turbines", Chalmers University of Technology, Ph.D. dissertation, Sweden, 2005.

35. Kostyantyn Protsenko and Dewei Xu, "Modeling and Control of Brushless Doubly-Fed Induction Generators in Wind Energy Applications", *IEEE Transactions on Power Electronics*, Vol. 23, No. 3, pp.1191- 1197, May 2008.

36. Yongchang Zhang, Zhengxi Li, Jiefeng Hu, Wei Xu and Jianguo Zhu, "A Cascaded Brushless Doubly Fed Induction Generator for Wind Energy Applications Based on Direct Power Control", *2011 International Conference on Electrical Machines and Systems* , pp.1-6, August 2011.

37. Istvan Erlich, Jörg Kretschmann, Jens Fortmann, Stephan Mueller-Engelhardt and Holger Wrede, "Modeling of Wind Turbine Based on Doubly-Fed Induction Generators for Power System Stability Studies", *IEEE Transactions on Power Systems*, Vol.22, No.3, pp. 909-919, August 2007.

38. Arantxa Tapia, Gerardo Tapia, J. Xabier Ostolaza and José Ramón Sáenz, "Modeling and Control of a Wind Turbine Driven Doubly Fed Induction Generator", *IEEE Transactions on Energy Conversion*, Vol. 18, No. 2, pp. 194-204, June 2003.

39. I. Erlich and F. Shewarega, "Modeling of Wind Turbines Equipped with Doubly-Fed Induction Machines for Power System Stability Studies", *2006 IEEE Power Systems Conference and Exposition*, pp. 978-985, November 2006.

40. Alvaro Luna, Francisco Kleber de Araujo Lima, David Santos, Pedro Rodríguez, Edson H. Watanabe, and Santiago Arnaltes, "Simplified Modeling of a DFIG for Transient Studies in Wind Power Applications", *IEEE Transactions on Industrial Electronics*, Vol. 58, No. 1, pp. 9-20, January 2011.

41. Katherine Elkington and Mehrdad Ghandhari, "Comparison of Reduced Order Doubly Fed Induction Generator Models for Nonlinear Analysis", *IEEE Electrical Power & Energy Conference*, pp.1-6, October 2009.

42. P. Sørensen, A. D. Hansen, T. Lund and H. Bindner, "Reduced Models of Doubly Fed Induction Generator System for Wind Turbine Simulations", *Wind Energy*, Vol. 9, No. 4, pp. 299-311, August 2006.

43. A. Samuel Neto, S. L. A. Ferreira, J. P. Arruda, F. A. S. Neves, P. A. C. Rosas and M. C. Cavalcanti, "Reduced Order Model for Grid Connected Wind Turbines with Doubly Fed Induction Generators", *IEEE International Symposium on Industrial Electronics*, pp. 2655-2660, June 2007.

44. Alireza Abbaszadeh, Saeed Lesan and Vahid Mortezapour, "Transient Response of Doubly Fed Induction Generator Under Voltage Sag Using an Accurate Model", *2009 IEEE PES/IAS Conference on Sustainable Alternative Energy (SAE)*, pp. 1-6, September 2009.

45. Pablo Ledesma and Julio Usaola, "Effect of Neglecting Stator Transients in Doubly Fed Induction Generators Models", *IEEE Transactions on Energy Conversion*, Vol. 19, No. 2, pp. 459-461, June 2004.

46. Torbjörn Thiringer and Jorma Luomi, "Comparison of Reduced-Order Dynamic Models of Induction Machines", *IEEE Transactions on Power Systems*, Vol.16, No. 1, pp. 119-126, February 2001.

47. Yan Guo, Xiao Wang, Howard C. Lee and Boon-Teck Ooi, "Pole-Placement Control of Voltage-Regulated PWM Rectifiers Through Real-Time Multiprocessing", *IEEE Transactions on Industrial Engineering*, Vol. 41, No. 2, pp. 224-230, April 1994.

48. José R. Rodríguez, Juan W. Dixon, José R. Espinoza, Jorge Pontt and Pablo Lezana, "PWM Regenerative Rectifiers: State of the Art", *IEEE Transactions on Industrial Electronics*, Vol. 52, No. 1, pp. 5-22, February 2005.

49. N. Horiuchi and T. Kawahito, "Torque and Power Limitations of Variable Speed Wind Turbines Using Pitch Control and Generator Power Control", *2001 Power Engineering Society Summer Meeting*, Vol. 1, pp. 638-643, July 2001.

50. Mohamed Mansour, M. N. Mansouri, and M. F. Mimouni, "Study of Performance of a Variable-Speed Wind Turbine with Pitch Control Based on a Permanent Magnet Synchronous Generator", *2011 8th International Multi-Conference on Systems, Signals & Devices*, pp. 1-6, March 2011.

51. Eduard Muljadi and C. P. Butterfield, "Pitch-Controlled Variable-Speed Wind Turbine Generation", *IEEE Transactions on Industry Applications*, Vol. 37, No. 1, pp. 240-246, February 2001.

52. Mohsen Faridi, Roghaiyeh Ansari, Seyed Ali Mousavi and Mahsa Dodman, "Pitch Control of Wind Turbine Blades in Noisy and Unstable Wind Conditions", *2010 9th International Conference on Environment and Electrical Engineering (EEEIC)*, pp. 22-25, May 2010.

53. Jianzhong Zhang, Ming Cheng, Zhe Chen and Xiaofan Fu, "Pitch Angle Control for Variable Speed Wind Turbines", *2008 Third International Conference on Electric Utility Deregulation and Restructuring and Power Technologies*, pp. 2691-2696, April 2008.

54. Tomonobu Senjyu, Ryosei Sakamoto, Naomitsu Urasaki, Toshihisa Funabashi, Hideki Fujita and Hideomi Sekine, "Output Power Leveling of Wind Turbine Generator for All Operating Regions by Pitch Angle Control", *IEEE Transactions on Energy Conversion*, Vol. 21, No. 2, pp. 467-475, June 2006.

55. E.B. Muhando, T. Senjyu, A. Yona, H. Kinjo and T. Funabashi, "Disturbance Rejection by Dual Pitch Control and Self-Tuning Regulator for Wind Turbine Generator Parametric Uncertainty Compensation", *IET Control Theory & Applications*, Vol. 1, No. 5, pp. 1431-1440, September 2007.

56. N. A. Schinas, N. A. Vovos and G. B. Giannakopoulos, "An Autonomous System Supplied Only by a Pitch-Controlled Variable-Speed Wind Turbine", *IEEE Transactions on Energy Conversion*, Vol. 22, No. 2, pp. 325- 331, June 2007.

57. I. Hamzaoui, F. Bouchafaa, A. Hadjammar and A. Talha, A. "Improvement of the Performances MPPT System of Wind Generation", *2011 Saudi*

International on Electronics, Communications and Photonics Conference, pp. 1-6, April 2011.

58. Shuhui Li, Timothy A. Haskew and Eduard Muljadi, "Integrative Characteristic Evaluation of DFIG Maximum Power Extraction using Lookup Table Approach", *2010 IEEE Power and Energy Society General Meeting*, pp. 1-8, July 2010.

59. H. Li, Z. Chen and John K. Pedersen, "Optimal Power Control Strategy of Maximizing Wind Energy Tracking and Conversion for VSCF Doubly Fed Induction Generator System", *IEEE 5th International Power Electronics and Motion Control Conference*, Vol.3, pp. 1-6, August 2006.

60. Mohamed Hilal, Mohamed Maaroufi and Mohamed Ouassaid, "Doubly Fed Induction Generator Wind Turbine Control for a maximum Power Extraction", *2011 International Conference on Multimedia Computing and Systems*, pp. 1-7, April 2011.

61. R. Pena, J. C. Clare and G. M. Asher, "Doubly fed induction generator using back-to-back PWM converters and its application to variable-speed wind-energy generation," *IEE Proceedings Electric Power Applications*, Vol. 143, No. 3, pp. 231-241, May 1996.

62. Y. Zhao, X. D. Zou, Y. N. Xu, Y. Kang and J. Chen, "Maximal Power Point Tracking under Speed-Mode Control for Wind Energy Generation System with Doubly Fed Introduction Generator", *IEEE 5th International Power Electronics and Motion Control Conference*, Vol.1, pp. 1-5, August 2006.

63. Xie Zhen, Zhang Xing, Yang Shuying, Li Qin and Zhai Wenfeng, "Study on Control Strategy of Maximum Power Capture For DFIG in Wind Turbine System", *2010 2nd IEEE International Symposium on Power Electronics Distributed Generation Systems*, pp. 110-115, June 2010.

64. Yunqi Xiao and Pengxiao Jia, "VSCF Wind Turbine Control Strategy for Maximum Power Generation", *Proceedings of the 8th World Congress on Intelligent Control and Automation*, Jinan, China, pp. 4781-4786, July 2010.

65. Rajib Datta and V. T. Ranganathan, "A Method of Tracking the Peak Power Points for a Variable Speed Wind Energy Conversion System", *IEEE Transactions on Energy Conversion*, Vol. 18, No. 1, pp. 163-168, March 2003.

66. Baike Shen, Bakari Mwinyiwiwa, Yongzheng Zhang and Boon-Teck Ooi, "Sensorless Maximum Power Point Tracking of Wind by DFIG Using Rotor Position Phase Lock Loop (PLL)", *IEEE Transactions on Power Electronics*, Vol. 24, No. 4, pp. 942-951, April 2009.

67. Changhong Shao, Xiangjun Chen and Zhonghua Liang. "Application Research of Maximum Wind energy Tracing Controller Based Adaptive Control Strategy in WECS", *IEEE 5th International Power Electronics and Motion Control Conference*, pp. 1-5, August 2006.

68. Eftichios Koutroulis and Kostas Kalaitzakis, "Design of a Maximum Power Tracking System for Wind-Energy-Conversion Applications", *IEEE Transactions on Industrial Electronics*, Vol. 53, No. 2, pp. 486-494, April 2006.

69. S. Chondrogiannis and M. Barnes, "Stability of Doubly-Fed Induction Generator Under Stator Voltage Orientated Vector Control", *IET Renewable Power Generation*, Vol. 2, No. 3, pp. 170-180, September 2008.

70. Carles Batlle, Arnau D`oria-Cerezo and Romeo Ortega, "A Stator Voltage Oriented PI Controller For The Doubly-Fed Induction Machine", *Proceedings of the 2007 American Control Conference*, New York City, USA, pp. 5438-5443, July 2007.

71. Shuhui Li, Rajab Challoo and Marty J. Nemmers, "Comparative Study of DFIG Power Control Using Stator-Voltage and Stator-Flux Oriented Frames", *IEEE Power & Energy Society General Meeting*, pp. 1-8, July 2009.

72. Jihen Arbi, Manel Jebali-Ben Ghorbal, Ilhem Slama-Belkhodja and Lotfi Charaabi, "Direct Virtual Torque Control for Doubly Fed Induction Generator Grid Connection", *IEEE Transactions on Industrial Electronics*, Vol. 56, No. 10, pp. 4163-4173, October 2009.

73. M. Tazil, V. Kumar, R. C. Bansal, S. Kong, Z. Y. Dong, W. Freitas and H. D. Mathur, "Three-phase doubly fed induction generators: an overview", *IET Electric Power Applications*, Vol. 4, No. 2, pp. 75-89, February 2010.

74. Domenico Casadei, Francesco Profumo, Giovanni Serra and AngeloTani, "FOC and DTC: Two Viable Schemes for Induction Motors Torque Control", *IEEE Transactions on Power Electronics*, Vol. 17, No. 5, pp. 779-787, September 2002.

75. K. C. Wong, S. L. Ho and K. W. E. Cheng, "Direct Torque Control of a Doubly-fed Induction Generator with Space Vector Modulation", *Electric Power Components and Systems*, Vol. 36, No. 12, pp. 1337-1350, November 2008.

76. F. Bonnet, P. E. Vidal and M. Pietrzak-David, "Direct Torque Control of Doubly Fed Induction Machine", *Bulletin of The Polish Academy of Sciences Technical Sciences*, Vol. 54, No. 3, pp. 307-314, 2006.

77. Z. Liu, O. A. Mohammed and S. Liu, "A Novel Direct Torque Control Induction Generator Used for Variable Speed Wind Power Generation", *IEEE Power Engineering Society General Meeting*, pp. 1-6, June 2007.

78. Etienne Tremblay, Sergio Atayde, and Ambrish Chandra, "Comparative Study of Control Strategies for the Doubly Fed Induction Generator in Wind Energy Conversion Systems: A DSP-Based Implementation Approach", *IEEE Transactions on Sustainable Energy*, Vol. 2, No. 3, pp. 288-299, July 2011.

79. Mariusz Malinowski, Marian P. Kazmierkowski and Andrzej M. Trzynadlowski, "A Comparative Study of Control Techniques for PWM Rectifiers in AC Adjustable Speed Drives", *IEEE Transactions on Power Electronics*, Vol. 18, No. 6, pp. 1390-1396, November 2003.

80. Rajib Datta and V. T. Ranganathan, "Direct Power Control of Grid-Connected Wound Rotor Induction Machine Without Rotor Position Sensors", *IEEE Transactions on Power Electronics*, Vol. 16, No. 3, pp. 390-399, May 2001.

81. David Santos-Martin, Jose Luis Rodriguez-Amenedo and Santiago Arnalte, "Direct Power Control Applied to Doubly Fed Induction Generator Under Unbalanced Grid Voltage Conditions", *IEEE Transactions on Power Electronics*, Vol. 23, No. 5, pp. 2328-2336, September 2008.

82. Gonzalo Abad, Miguel A´ngel Rodr´ıguez, Grzegorz Iwanskiand and Javier Poza, "Direct Power Control of Doubly-Fed-Induction-Generator-Based Wind Turbines Under Unbalanced Grid Voltage", *IEEE Transactions on Power Electronics*, Vol. 25, No. 2, pp. 442-452, February 2010.

83. Lie Xu and Phillip Cartwright, "Direct Active and Reactive Power Control of DFIG for Wind Energy Generation", *IEEE Transactions on Energy Conversion*, Vol. 21, No. 3, pp. 750-758, September 2006.

84. Mostafa Soliman, O. P. Malik, and David T. Westwick, "Multiple Model Predictive Control for Wind Turbines With Doubly Fed Induction Generators", *IEEE Transactions on Sustainable Energy*, Vol. 2, No. 3, pp. 215- 225, July 2011.

85. Dawei Zhi, Lie Xu and Barry W. Williams, "Model-Based Predictive Direct Power Control of Doubly Fed Induction Generators", *IEEE Transactions On Power Electronics*, Vol. 25, No. 2, pp. 341-351, February 2010.

86. Lie Xu, Dawei Zhi and Barry W. Williams, "Predictive Current Control of Doubly Fed Induction Generators", *IEEE Transactions on Industrial Electronics*, Vol. 56, No. 10, pp. 4143-4153, October 2009.

87. Jiefeng Hu, Jianguo Zhu and D. G. Dorrell, "A Comparative Study of Direct Power Control of AC/DC Converters for Renewable Energy Generation", *37th Annual Conference on IEEE Industrial Electronics Society*, pp. 3578-3583, November 2011.

88. B. Hopfensperger, D. J. Atkinson and R. A. Lakin, "Stator-flux-oriented control of a doubly-fed induction machine with and without position encoder", *IEEE Proceedings Electric Power Applications*, Vol.147, No. 4, pp. 241-250, July 2000.

89. Sheng Yang and Venkataramana Ajjarapu, "A Speed-Adaptive Reduced-Order Observer for Sensorless Vector Control of Doubly Fed Induction Generator-Based Variable-Speed Wind Turbines", *IEEE Transactions on Energy Conversion*, Vol. 25, No. 3, pp. 891-900, September 2010.

90. G. D. Marques, V. Fern˜ao Pires, S´ergio Sousa and Duarte M. Sousa, "A DFIG Sensorless Rotor-Position Detector Based on a Hysteresis Controller", *IEEE Transactions On Energy Conversion*, Vol. 26, No. 1, pp. 9-17, March 2011.

91. Ralph Teichmann and Steffen Bernet, "A Comparison of Three-Level Converters versus Two-Level Converters for Low-Voltage Drives, Traction, and Utility Applications", *IEEE Transactions on Industry Applications*, Vol. 41, No. 3, pp. 855-865, May/June 2005.